HHS Public Access

Author manuscript

Cell Rep. Author manuscript; available in PMC 2023 October 23.

Published in final edited form as:

Cell Rep. 2023 February 28; 42(2): 112103. doi:10.1016/j.celrep.2023.112103.

Nitric oxide suppression by secreted frizzled-related protein 2 drives retinoblastoma

Panneerselvam Jayabal[1], **Fuchun Zhou**[1], **Xiuye Ma**[1], **Kathryn M. Bondra**[1], **Barron Blackman**[1], **Susan T. Weintraub**[2,3], **Yidong Chen**[1,3,4], **Patricia Chévez-Barrios**[5], **Peter J. Houghton**[1,3,6], **Brenda Gallie**[7], **Yuzuru Shiio**[1,2,3,8,*]

[1]Greehey Children's Cancer Research Institute, The University of Texas Health Science Center, San Antonio, TX 78229, USA

[2]Department of Biochemistry and Structural Biology, The University of Texas Health Science Center, San Antonio, TX 78229, USA

[3]Mays Cancer Center, The University of Texas Health Science Center, San Antonio, TX 78229, USA

[4]Department of Population Health Sciences, The University of Texas Health Science Center, San Antonio, TX 78229, USA

[5]Department of Pathology and Genomic Medicine, Houston Methodist Hospital, Houston, TX 77030, USA

[6]Department of Molecular Medicine, The University of Texas Health Science Center, San Antonio, TX 78229, USA

[7]The Hospital for Sick Children, 555 University Avenue, Toronto, ON M5G 1X8, Canada

[8]Lead contact

SUMMARY

Retinoblastoma is a cancer of the infant retina primarily driven by loss of the Rb tumor suppressor gene, which is undruggable. Here, we report an autocrine signaling, mediated by secreted frizzled-related protein 2 (SFRP2), which suppresses nitric oxide and enables retinoblastoma growth. We show that coxsackievirus and adenovirus receptor (CXADR) is the cell-surface receptor for SFRP2 in retinoblastoma cells; that CXADR functions as a "dependence receptor," transmitting a growth-inhibitory signal in the absence of SFRP2; and that the balance between SFRP2 and CXADR determines nitric oxide production. Accordingly, high SFRP2 RNA expression correlates

*Correspondence: shiio@uthscsa.edu.

AUTHOR CONTRIBUTIONS

P.J., F.Z., and Y.S. designed the research. P.J., F.Z., X.M., K.M.B., B.B., S.T.W., Y.C., P.C.-B., P.J.H., and Y.S. performed the research. P.J., F.Z., K.M.B., B.B., S.T.W., Y.C., P.C.-B., P.J.H., and Y.S. analyzed the data. B.G. provided retinoblastoma cell lines and advice regarding the course of the project. Y.S. wrote the paper with input from other authors.

DECLARATION OF INTERESTS

The authors declare no competing interests.

SUPPLEMENTAL INFORMATION

Supplemental information can be found online at https://doi.org/10.1016/j.celrep.2023.112103.

with high-risk histopathologic features in retinoblastoma. Targeting SFRP2 signaling by SFRP2-binding peptides or by a pharmacological inhibitor rapidly induces nitric oxide and profoundly inhibits retinoblastoma growth in orthotopic xenograft models. These results reveal a cytokine signaling pathway that regulates nitric oxide production and retinoblastoma cell proliferation and is amenable to therapeutic intervention.

Graphical Abstract

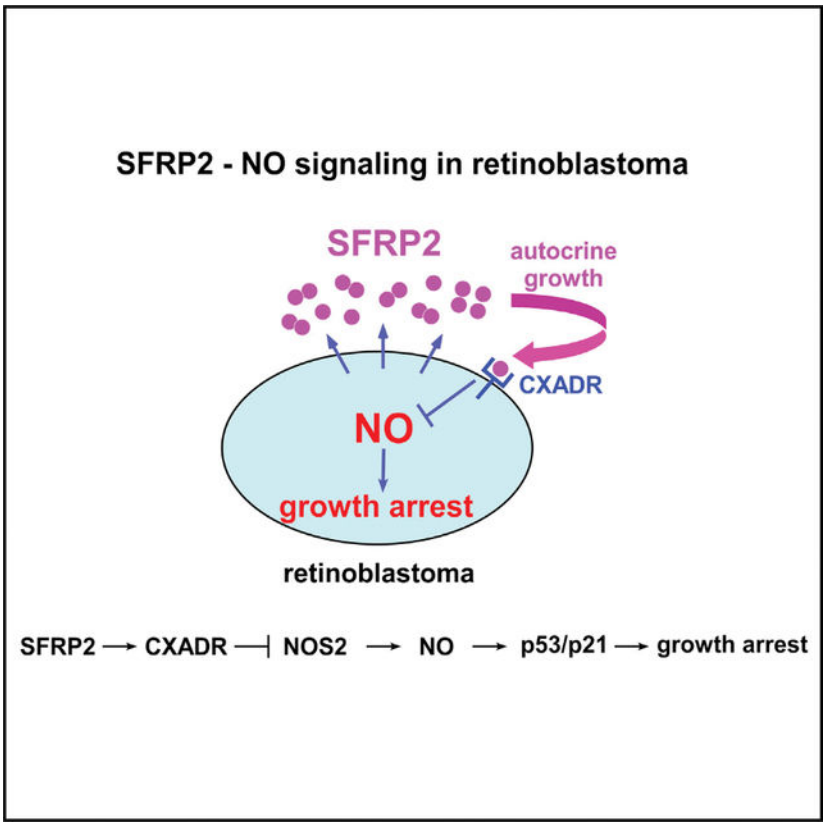

In brief

Nitric oxide plays critical roles in vasodilation and neurotransmission, but little is known about the role of nitric oxide in tumorigenesis and extracellular signaling that regulates nitric oxide. Jayabal et al. report that SFRP2-CXADR signaling suppresses nitric oxide and drives retinoblastoma.

INTRODUCTION

Nitric oxide is a gaseous messenger molecule originally identified as the endothelium-derived relaxing factor.[1–3] It has a variety of biological functions, such as vasodilation, neurotransmission, and immune response. Nitric oxide is synthesized from arginine by the action of three isoforms of nitric oxide synthases (NOSs): neural, inducible, and endothelial NOS (nNOS/NOS1, iNOS/NOS2, and eNOS/NOS3, respectively). Nitric oxide stimulates soluble guanylate cyclase (sGC), which generates cGMP. cGMP, in turn, stimulates cGMP-dependent protein kinase (PKG). This enzyme cascade is considered

the canonical signaling mechanism for nitric oxide.[4] In contrast to its critical roles in vasodilation and neurotransmission, nitric oxide has not emerged as a key regulator of tumorigenesis. Importantly, little is known about extracellular signaling that regulates nitric oxide production.

Retinoblastoma is a cancer of the infant retina primarily caused by biallelic inactivation of the Rb tumor suppressor gene.[5,6] Inheritance of one mutant Rb allele predisposes individuals to retinoblastoma, which forms after the second Rb allele is mutated. Mutations in genes other than Rb are rare.[7,8] If retinoblastoma is detected early, then enucleation is often curative, but this inevitably results in vision loss. To save vision, chemotherapy is commonly used, but is often associated with short-term and long-term toxicity.[5] Despite years of research, there is no molecularly targeted therapy for retinoblastoma.

Unlike human retinoblastoma, Rb inactivation is not sufficient to generate retinoblastoma in mice. Retinoblastoma mouse models require an additional mutation of Rb paralogs (p107 or p130) or a CDK inhibitor, p27, in conjunction with Rb loss[9–14] and are derived from the amacrine lineage,[15] unlike human retinoblastoma, which appears to be derived from cone precursor cells.[16,17] Previous research on retinoblastoma has predominantly focused on intracellular pathways. Little is known about extracellular signaling that regulates retinoblastoma.

Secreted frizzled-related protein 2 (SFRP2) is a multi-functional cytokine that is implicated in retinal neurogenesis[18] and also serves as an axon guidance cue for developing retinal neurons.[19] SFRP2 knockout mice display abnormal navigation of retinal axons, which is worsened in SFRP2/SFRP1 double-knockout mice.[20] SFRP2 is known to function as a Wnt antagonist and tumor suppressor. SFRP2 can directly bind Wnt and prevent Wnt binding to its receptor, Frizzled.[21] SFRP2 gene expression is frequently silenced by promoter methylation in a variety of human cancers,[22,23] consistent with the role of SFRP2 as a tumor suppressor. However, there are also several studies demonstrating a tumor-promoting role of SFRP2.[24,25]

In this study, we describe an SFRP2-nitric oxide signaling pathway that controls retinoblastoma growth. Our results indicate that SFRP2 uses coxsackievirus and adenovirus receptor (CXADR) as the receptor and prevents production of nitric oxide. Targeting SFRP2 results in rapid production of nitric oxide, which potently inhibits retinoblastoma growth.

RESULTS

Retinoblastoma depends on SFRP2

To dissect cytokine signaling in retinoblastoma, we analyzed the proteins secreted from Y79 and RB383 retinoblastoma cells by mass spectrometry. The complete lists of proteins identified with high confidence are shown in Tables S1 and S2. This analysis identified abundant secretion of SFRP2 (Tables S1 and S2). SFRP2 secretion was not detected in the secretome of other childhood cancers, including osteosarcoma, Ewing sarcoma, synovial sarcoma, rhabdomyosarcoma, neuroblastoma, and hepatoblastoma.[26,27] SFRP2 is highly expressed in all five retinoblastoma cell lines and five retinoblastoma tumors tested (Figure

1A). By contrast, SFRP2 expression is low or undetectable in ARPE-19 retinal pigment epithelial cells, mesenchymal stem cells, rhabdomyosarcoma cells, Ewing sarcoma cells, and normal tonsils (Figure 1A).

Importantly, silencing of SFRP2 by small interfering RNA (siRNA) transfection severely inhibited proliferation of all five retinoblastoma cell lines tested but did not affect ARPE-19 and 293T/HEK293T cell proliferation (Figure 1B; Dharmacon SFRP2 SMARTpool siRNAs; proliferation assessed by the IncuCyte live-cell imagingsystem). SFRP1 siRNA SMART pool didnot affect retinoblastoma growth (Figure 1B). SFRP2 silencing also caused apoptosis in retinoblastoma cells (Figures 1C and 1D), suggesting that SFRP2 silencing is both cytostatic and cytocidal. Additionally, an anti-SFRP2 rabbit polyclonal antibody inhibited retinoblastoma cell proliferation in a dose-dependent manner (Figure 1E). Retinoblastoma growth inhibition by SFRP2 siRNA was rescued by adding recombinant SFRP2 (R&D Systems, 6838-FR/CF, used at 250 ng/mL) to the culture medium (Figure 1F), indicating that retinoblastoma depends on extracellular SFRP2. Furthermore, SFRP2 silencing strongly inhibited the xenograft tumorigenicity of retinoblastoma cells (Figure 1G). These results demonstrate that retinoblastoma depends on SFRP2.

The analysis of published gene expression data on retinoblastoma tumors[28] revealed that tumors with high-risk histopathologic features (HRPFs), which are associated with worse prognosis and indicate the need for adjuvant chemotherapy after enucleation,[30–32] display significantly higher SFRP2 RNA expression levels than tumors without HRPFs (Figure 1H).

We also performed immunohistochemistry of retinoblastoma tumors and found that retinoblastoma tumors are positive for SFRP2, although the intensity of SFRP2 staining does not seem to correlate with invasiveness (non-invasive, PLONI [post-laminar optic nerve invasion], and PLONI + massive choroidal invasion) (Table S3). The lack of correlation might be due to the fact that immunohistochemistry detects SFRP2 retained in cells, not secreted SFRP2.

SFRP2 silencing triggers nitric oxide (NO) production, which inhibits retinoblastoma growth

To gain insight into downstream signaling, we analyzed changes in gene expression induced by SFRP2 silencing in RB383 cells by RNA sequencing and Ingenuity Pathway Analysis, which identified NOS signaling as a top canonical pathway 24 h (Figure 2A), CREB1 as a top upstream regulator 24 h (Figure 2B), and p53 and p21 as top upstream regulators 48 h after SFRP2 siRNA transfection (Figure 2C). We then analyzed NO production upon SFRP2 siRNA transfection using nitrate/nitrite colorimetric assays and observed rapid NO production that peaked 12 h after SFRP2 siRNA transfection (Figures 2D and S1A; analyzed both in the conditioned medium [CM] and cell lysate). Furthermore, we found rapid induction of NOS2 (iNOS) and NOS3 (eNOS) proteins (Figures 2E and S1B) upon SFRP2 silencing.

We then evaluated the role of NO in mediating growth inhibition in retinoblastoma. An NO scavenger, carboxy-PTIO, completely abolished SFRP2 silencing-induced growth inhibition in all five retinoblastoma cell lines (Figure 2F). Carboxy-PTIO did not affect

SFRP2 silencing (Figure 2G). A pan-NOS inhibitor, L-NMMA, also abolished growth inhibition following SFRP2 silencing (Figure 2H). Conversely, an NO donor, SNAP, inhibited retinoblastoma growth in a dose-dependent manner (Figure 2I). These results indicate that NO mediates growth inhibition following SFRP2 silencing in retinoblastoma.

NO activates sGC, which generates cGMP, leading to activation of PKG. This pathway is considered the major mode of action for NO and mediates a variety of its biological functions, including smooth muscle relaxation. We found that SFRP2-silencing-induced growth inhibition of retinoblastoma cells is abolished by an inhibitor of sGC, NS-2028 (Figure 2J), and an inhibitor of PKG, KT5823 (Figure 2K), indicating that the NO-sGC-PKG pathway mediates growth inhibition that results from SFRP2 silencing.

SFRP2 silencing was accompanied by activation of the p53-p21 pathway (Figure 2C), and we found that growth inhibition following SFRP2 silencing is abolished by simultaneous silencing of p53 or p21 (Figure 2L), indicating that SFRP2 silencing results in p53- and p21-dependent growth inhibition in retinoblastoma. p21 induction following SFRP2 silencing was abolished by carboxy-PTIO, NS-2028, and KT5823 (Figure 2M), indicating that the NO-sGC-PKG pathway induces p21 in retinoblastoma.

These results suggest that SFRP2 normally prevents NO production in retinoblastoma and that SFRP2 silencing results in NO production and p53- and p21-dependent growth arrest through the NO-sGC-PKG pathway (Figure 2N).

The RNA expression data in the Human Protein Atlas (www.proteinatlas.org) demonstrates high SFRP2 expression in AF22 neural stem cells.[33] We confirmed that AF22 cells indeed express high levels of SFRP2, comparable with those in retinoblastoma cells (Figure S2A). SFRP2 silencing (Figure S2B) resulted in rapid production of NO (Figure S2C) and growth inhibition (Figure S2D) in AF22 cells. These results suggest that SFRP2-NO signaling also regulates proliferation (self-renewal) of AF22 neural stem cells.

The adenylate cyclase-PKA-CREB-NOS2 pathway mediates NO production following SFRP2 silencing

While both NOS2 and NOS3 were induced upon SFRP2 silencing in retinoblastoma (Figures 2E and S1B), silencing of NOS2 completely abrogated and that of NOS3 partly affected NO production and growth inhibition following SFRP2 silencing (Figures 3A–3C). Unlike NOS1 and NOS3, NOS2 enzymatic activity is not regulated by intracellular calcium, and induction of NOS2 expression readily translates into increased NOS activity. Similar to NOS2 protein levels (Figure 2E), NOS2 RNA levels rapidly increased upon SFRP2 siRNA transfection (Figure 3D).

NOS2 expression can be activated by CREB[34] and cyclic AMP (cAMP).[35,36] Ingenuity Pathway Analysis of SFRP2-silenced RB383 cells identified CREB1 as the top upstream regulator 24 h after SFRP2 siRNA transfection (Figure 2B). We found that phosphorylation of CREB is rapidly induced upon SFRP2 siRNA transfection in retinoblastoma cells (Figure 3E). CREB silencing (Figure 3I) abrogated NOS2 induction (Figure 3F), NO production

(Figure 3G), and growth inhibition (Figure 3H) following SFRP2 silencing, indicating the role of CREB in these processes.

CREB is phosphorylated and activated by cAMP-dependent protein kinase (PKA). The PKA inhibitor H89 abolished CREB phosphorylation (Figure 3J), NOS2 induction (Figure 3K), NO production (Figure 3L), and growth inhibition (Figure 3M) following SFRP2 silencing. PKA is activated by cAMP produced by adenylate cyclase. The adenylate cyclase inhibitor NKY80 abolished NOS2 induction (Figure 3N), NO production (Figure 3O), and growth inhibition (Figure 3P) following SFRP2 silencing.

These results suggest that the adenylate cyclase-PKA-CREB-NOS2 pathway mediates NO production and growth arrest following SFRP2 silencing in retinoblastoma (Figure 3Q).

CXADR functions as the SFRP2 dependence receptor in retinoblastoma

SFRP2 functions as a Wnt antagonist and tumor suppressor. SFRP2 can directly bind Wnt and prevent Wnt binding to its receptor, Frizzled.[21] SFRP2 gene expression is frequently silenced by promoter methylation in various human cancers.[22,23] We initially thought that SFRP2's role as a Wnt antagonist is important in retinoblastoma. However, pharmacological inhibitors of Wnt signaling (XAV939 for canonical [Wnt/β-catenin] signaling and IWP-L6 [inhibitor of Wnt lipidation and secretion] for canonical and non-canonical signaling; both used at 1 μM) did not rescue the growth arrest of retinoblastoma cells following SFRP2 silencing (Figures S3A and S3B). Furthermore, silencing of β-catenin inhibited, not stimulated, retinoblastoma proliferation (Figure S3C). These results suggest that Wnt antagonism by SFRP2 is unlikely to play a growth-promoting role in retinoblastoma. We thus started to search for a cell-surface receptor of SFRP2.

To analyze the retinoblastoma cell surface proteome, we used cell-surface labeling with a membrane-impermeable biotin derivative (EZ-Link Sulfo-NHS-SS-Biotin, Pierce/Thermo Fisher Scientific), followed by purification with streptavidin agarose and mass spectrometry. The complete lists of proteins identified with high confidence are shown in Tables S4 and S5. This analysis revealed that CXADR is highly expressed on the retinoblastoma cell surface (RB383: 64 peptides, 56.7% sequence coverage; Y79: 37 peptides, 62.2% sequence coverage). CXADR is a transmembrane protein that functions as a virus receptor and a component of tight junctions.[37,38] CXADR mRNA is highly expressed in retinoblastoma cell lines and tumors compared with ARPE-19 retinal pigment epithelial cells (Figure 4A). In line with this finding, a recent study, which demonstrated the therapeutic efficacy of an oncolytic adenovirus against retinoblastoma, reported high CXADR expression in retinoblastoma tumors compared with surrounding normal tissues.[39]

We first tested the physical interaction between SFRP2 and CXADR by co-immunoprecipitation; transfected SFRP2 specifically co-immunoprecipitated with CXADR in 293T cells (Figure 4B). We then used ligand-binding assays. C-terminally FLAG-tagged SFRP2 was produced by transfection in 293T cells and incubated with Y79 cells. After washing the cells to remove unbound SFRP2, cells were lysed, and SFRP2-FLAG binding to Y79 cells was assessed by anti-FLAG immunoblotting. As shown in Figure 4C, SFRP2-FLAG bound to Y79 cells, and this binding was abolished by siRNA-mediated silencing

of CXADR, indicating that CXADR is the SFRP2 receptor in retinoblastoma cells. Using microscale thermophoresis, we determined the K_D of interaction between recombinant SFRP2 and recombinant CXADR (3336-CX-05, R&D Systems) to be 11.9 nM (Figure 4D).

We then assessed the functional interaction between SFRP2 and CXADR. Growth inhibition following SFRP2 silencing was abolished by simultaneous silencing of CXADR; CXADR silencing alone had no effect on proliferation (Figure 4E). This suggests that CXADR functions as a "dependence receptor," transmitting inhibitory signals in the absence of its ligand, SFRP2.

Rescue of SFRP2 silencing-induced growth inhibition by simultaneous silencing of CXADR (Figure 4E) was accompanied by abrogation of CREB phosphorylation (Figure 4F) and NO generation (Figure 4G). Furthermore, lentiviral overexpression of CXADR inhibited retinoblastoma growth (Figure 4H), accompanied by NO generation (Figure 4I). Interestingly, NO generation in CXADR-overexpressing cells was rapidly abolished when we added recombinant SFRP2 to the culture medium (Figure 4I), which was accompanied by the rescue of proliferation (Figure 4J).

Importantly, we were able to recapitulate the opposing activities of CXADR and SFRP2 in NO regulation by transfection in 293T cells. Transfection of CXADR in 293T cells induced cAMP, phosphorylated CREB, NOS2, and NO production, which was blocked by co-transfection of SFRP2 (Figures S4A–S4E), underscoring the antagonistic activities displayed by SFRP2 and CXADR. A recent interactome proteomics study identified the interaction between CXADR and adenylate cyclase 9 (ADCY9),[40] which might mediate the regulation of cAMP production by CXADR.

These results suggest that the balance between SFRP2 and CXADR determines NO production (Figure 4K). Under normal growth conditions, SFRP2 is abundantly secreted from retinoblastoma, which binds CXADR and prevents NO production (Figure 4K, 1). SFRP2 silencing triggers NO production through CXADR, leading to growth arrest (Figure 4K, 2). When both SFRP2 and CXADR are silenced, NO production is not induced, and retinoblastoma can proliferate (Figure 4K, 3). CXADR silencing alone does not induce NO production and allows retinoblastoma proliferation (Figure 4K, 4).

Targeting SFRP2 signaling in retinoblastoma

To identify peptides that bind SFRP2 and block SFRP2 signaling, we screened the phage display library with recombinant SFRP2 protein. Random 12-mer peptides fused to the pIII phage coat protein through a flexible GGGS linker were expressed on the surface of M13 phages, and the library of peptide-expressing phages was incubated with recombinant SFRP2 protein. After three cycles of binding, washing, and phage amplification, the phage inserts encoding the 12-mer peptides were sequenced. From this, we identified the HNPFTFFGPMFY peptide (which we termed peptide I) 9 times and the HGWASLLNYSWY peptide (termed peptide II) 4 times among 30 phage clones sequenced (Figure 5A). Peptides I and II bound to full-length SFRP2 and the C-terminal netrin domain of SFRP2 (Figure 5B). Furthermore, peptides I and II rapidly induced phosphorylated CREB

(Figure 5C), NOS2 (Figure 5D), and NO production (Figure 5E) and strongly inhibited proliferation of retinoblastoma cells (Figure 5F). The SFRP2-binding peptides did not inhibit the growth of ARPE-19 retinal pigment epithelial cells (Figure 5G), suggesting selective toxicity against retinoblastoma.

Screening of a chemical library for compounds that block SFRP1-mediated inhibition of the Wnt/β-catenin reporter led to identification of WAY-316606 as a potent inhibitor of SFRP1, which also binds to SFRP2 (SFRP2-WAY-316606 K_D = 1 μM).[41] WAY-316606 blocks the Wnt repression activity of full-length SFRP1 but not the SFRP1 N-terminal cysteine-rich domain lacking the C-terminal netrin domain, which suggested that the target of WAY-316606 is the C-terminal netrin domain.[41] We found that WAY-316606 rapidly induces NO generation in retinoblastoma cells (Figure 5H). Furthermore, WAY-316606 efficiently inhibited retinoblastoma cell proliferation in a dose-dependent manner (Figure 5I). Importantly, WAY-316606 did not affect the growth of ARPE-19 retinal pigment epithelial cells (Figure 5J), suggesting its selective toxicity against retinoblastoma.

To better mimic retinoblastoma patient tumors, we established orthotopic xenograft models by injecting luciferase-expressing retinoblastoma cells into the vitreous bodies of severe combined immunodeficiency (SCID) mice (Figure 6A). Using these orthotopic xenograft models, we were able to show that tumor growth in these models depends on SFRP2 (Figures 6A and 6B).

We also used orthotopic xenograft models to evaluate the efficacy of SFRP2-binding peptides and WAY-316606. We found that a one-time injection of SFRP2-binding peptide II significantly inhibits orthotopic tumor growth (Figure 6C). Furthermore, four-time repeated injections of SFRP2-binding peptide II and WAY-316606 significantly inhibited orthotopic tumor growth (Figure 6D).

Collectively, these results suggest that the SFRP2 dependence of retinoblastoma is amenable to therapeutic targeting.

DISCUSSION

In this study, we uncovered a cytokine signaling pathway that controls NO production and retinoblastoma growth. Using secretome proteomics, we found that retinoblastoma abundantly secretes SFRP2 and demonstrated that retinoblastoma depends on the autocrine signaling mediated by SFRP2 (Figure 1). Regarding downstream signaling, we determined that silencing of SFRP2 results in rapid production of NO, leading to p53-dependent growth arrest of retinoblastoma (Figure 2). We also found that the adenylate cyclase-PKA-CREB-NOS2 pathway mediates NO production upon SFRP2 silencing (Figure 3). Employing cell-surface proteomics, we found that CXADR is highly expressed on the surface of retinoblastoma cells and demonstrated that CXADR functions as the SFRP2 dependence receptor, triggering NO production in the absence of SFRP2 (Figure 4). Using SFRP2-binding peptides and a pharmacological inhibitor, we demonstrated the feasibility of targeting SFRP2 signaling in retinoblastoma (Figures 5 and 6).

We found that high SFRP2 RNA expression correlates with the presence of HRPFs in retinoblastoma tumors (Figure 1H), which are associated with poorer prognosis and indicate the need for adjuvant chemotherapy after enucleation.[30–32] This result suggests that SFRP2 RNA expression levels can be used as a biomarker for high-risk retinoblastoma. Currently, the clinical risk of retinoblastoma is estimated by a combination of clinical and histopathological features.[5,28] SFRP2 RNA expression levels can be used in the future to more precisely identify high-risk retinoblastoma tumors and guide therapy decision making, in conjunction with high-risk clinical and histopathologic features.

SFRP2 has been mainly studied as a Wnt antagonist and a tumor suppressor that is frequently silenced by promoter methylation in multiple cancer types.[22,23] This study uncovered a tumor-promoting function for SFRP2: a ligand of CXADR, preventing NO production and growth arrest in retinoblastoma. The critical role of NO in mediating growth arrest upon SFRP2 silencing was established by the rescue of growth arrest by an NO scavenger, carboxy-PTIO (Figure 2F), and a pan-NOS inhibitor, L-NMMA (Figure 2H), as well as dose-dependent growth inhibition by an NO donor, SNAP (Figure 2I). Furthermore, the downstream targets of NO, sGC and PKG, play essential roles in SFRP2 silencing-induced growth arrest (Figures 2J and 2K). While NO has well-established roles in blood vessel dilation and neurotransmission, its role in cancer is less well understood. We envision that the SFRP2-NO signaling pathway in retinoblastoma will provide a useful model to study the role of NO in cancer. Because of the long history of NO research, there are a number of reagents available to manipulate NO signaling, which will likely facilitate therapeutic targeting of SFRP2-NO signaling in retinoblastoma.

In addition, our data indicate that SFRP2-NO signaling also plays an important role in neural stem cells. AF22 neural stem cells express high levels of SFRP2, comparable with retinoblastoma cells, and silencing of SFRP2 resulted in rapid induction of NO production and inhibition of proliferation (self-renewal) of these neural stem cells (Figures S2A–S2D). Thus, the biological role of SFRP2-NO signaling is not limited to retinoblastoma. It will be interesting to explore the role of SFRP2-NO signaling in other types of stem cells and cancers.

CXADR was originally identified as a receptor for coxsackievirus and adenovirus using biochemical purification[42] and phage expression library screening.[43] CXADR is highly expressed in retinoblastoma tumors,[39] which motivated use of an oncolytic adenovirus, VCN-01, as a potential therapy for retinoblastoma. VCN-01 demonstrated anti-retinoblastoma efficacy *in vitro*, in mice, and in a phase 1 clinical trial.[39] In light of the present finding, part of the anti-retinoblastoma effect of VCN-01 can be mediated by blockade of the SFRP2-CXADR interaction. Additionally, adenovirus vectors can be devised to simultaneously target SFRP2-NO signaling and SFRP2-CXADR interaction in retinoblastoma.

Limitations of the study

Although this study revealed the SFRP2-NO signaling pathway, the mechanistic details of some of the steps of the pathway remain to be clarified, including how CXADR regulates cAMP production and how PKG activates the p53-p21 axis. This study used retinoblastoma

cell lines and mouse xenograft models, which have inherent limitations in recapitulating human disease. Established cell lines grown under non-physiological culture conditions may not faithfully mimic retinoblastoma tumor cells in human patients. While we used orthotopic xenografts to model retinoblastoma, these models were made in immunodeficient mice and do not reflect the immune environment of human retinoblastoma tumors. Genetically engineered mouse models for retinoblastoma can be established in immuno-competent mice, but these models require an additional mutation of Rb paralogs (p107 or p130) or a CDK inhibitor, p27, in conjunction with Rb loss.[9–14] Tumor cells in these genetic mouse models are derived from the amacrine lineage,[15] unlike human retinoblastoma, which appears to be derived from cone precursor cells.[16,17] Therefore, these genetic models also have their own limitations. Although it is important to keep the limitations of the study in mind, the SFRP2 dependence of retinoblastoma uncovered by this study provides an excellent opportunity for therapeutic targeting. It will now be important to evaluate the approaches to target SFRP2-CXADR-NO signaling in retinoblastoma patients to develop a much-needed targeted therapy.

STAR★METHODS

Detailed methods are provided in the online version of this paper and include the following:

RESOURCE AVAILABILITY

Lead contact—Further information and requests for resources and reagents should be directed to and will be fulfilled by the Lead Contact, Yuzuru Shiio (shiio@uthscsa.edu).

Materials availability—Plasmids generated in this study are available from the lead contact.

Data and code availability

- The mass spectrometry proteomics data have been deposited to the ProteomeXchange Consortium via the PRIDE [1] partner repository with the dataset identifier PXD039515 (Y79 secretome), PXD039516 (RB383 secretome), PXD039517 (Y79 cell surface proteome), and PXD039518 (RB383 cell surface proteome). The RNA-sequencing data were deposited in the GEO database (the accession number: GSE161990).
- This paper does not report original code.
- Any additional information required to reanalyze the data reported in this paper is available from the lead contact upon request.

EXPERIMENTAL MODEL AND SUBJECT DETAILS

Animals—Female 5 – 6 week old C.B.17SC scid−/− mice were used. All mice were housed in a pathogen-free vivarium in the University of Texas Health Science Center at San Antonio. Mice were randomly allocated to treatment groups. Blinding of the researcher measuring tumor size was employed. The animal research method was reviewed and

approved for humaneness by the Institutional Animal Care and Use Committee of the University of Texas Health Science Center at San Antonio.

Cell lines—Y79 cells were cultured in RPMI-1640 medium supplemented with 10% fetal bovine serum. RB383, RB247, RB409, and WERI-Rb-1 cells were cultured in Iscove's modified Dulbecco's medium (IMDM) supplemented with 10% fetal bovine serum, 10 μg/mL insulin, and 55 μM β-mercaptoethanol. ARPE-19 cells were cultured in Dulbecco's modified Eagle's medium/Nutrient Mixture F-12 (DMEM/F-12) supplemented with 10% fetal bovine serum. 293T cells were cultured in Dulbecco's modified Eagle's medium (DMEM) supplemented with 10% fetal bovine serum.

AF22 cells were cultured in DMEM/F-12 medium supplemented with 20% KSR, 10 μL/ml N-2 supplement (Thermo Fisher Scientific), 1 μL/ml B-27 supplement (Thermo Fisher Scientific), 10 ng/mL of bFGF (PeproTech), and 10 ng/mL of FGF (PeproTech), and the culture medium was replaced every second day. AF22 cells were plated on tissue culture plates coated with 0.1 mg/mL poly-L-ornithine (Sigma-Aldrich) and 10 μg/mL laminin (Sigma-Aldrich). The cell lines were STR-authenticated and were routinely tested for the absence of mycoplasma.

METHOD DETAILS

Transfection and viral infection—Calcium phosphate co-precipitation was used for transfection of 293T cells. Lentiviruses were prepared by transfection in 293T cells following System Biosciences' protocol, and the cells infected with lentiviruses were selected with 5 μg/mL puromycin for 48 h. cDNAs for SFRP2 and CXADR were cloned into pcDNA3 mammalian expression vector (Invitrogen/Thermo Fisher) or pCDH1-puro lentiviral expression vector (System Biosciences). The target sequences for shRNAs are as follows: SFRP2 shRNA-1, GAAGGA GATAACCTACATCAA; SFRP2 shRNA-2, GCAAGACCATTTACAAGCTGA; β-catenin shRNA, GCTTGGAATGAGACTGCTGAT; and control shRNA, CCTAAGGTTAAGTCGCCCTCG. The following siRNAs were used: human SFRP2 siRNA SMARTpool (M-024062-02, Dharmacon), human SFRP1 siRNA SMARTpool (M-004600-02, Dharmacon), human CXADR siRNA SMARTpool (M-003650-01, Dharmacon), human p21 siRNA SMARTpool (M-003471-00, Dharmacon), human p53 siRNA SMARTpool (M-003329-03, Dharmacon), human NOS2 siRNA SMARTpool (M-009240-01, Dharmacon), human NOS3 siRNA SMARTpool (M-006490-00, Dharmacon), human CREB1 siRNA SMARTpool (M-003619-01, Dharmacon), and Non-Targeting siRNA Pool #2 (D-001206-14-05; Dharmacon). Lipofectamine RNAiMAX Transfection Reagent (Thermo Fisher) was used for siRNA transfection.

Protein sample preparation and proteomic analysis—The preparation of secreted protein samples, mass spectrometry analysis, and proteomics data processing were performed essentially as described.[26,44] Cells were washed six times with culture medium without serum. Subsequently, cells were cultured in medium without serum for 24 h and the culture supernatant was harvested. The supernatant was centrifuged, filtered through a 0.45-μm filter (Millipore), and concentrated using 3,000-Da cut-off Amicon Ultra Centrifugal

Filter Units (Millipore). Biotinylation of cell surface proteins by EZ-Link Sulfo-NHS-SS-Biotin (Pierce/Thermo Fisher) and isolation of biotinylated proteins were carried out as described.[45] The proteins in each sample were fractionated by SDS-PAGE and visualized by Coomassie blue. Each gel lane was divided into six slices, and the proteins in each slice were digested *in situ* with trypsin (Promega; sequencing grade) in 40 mM NH_4HCO_3 overnight at 37°C. The resulting tryptic peptides were analyzed by HPLC-ESI-tandem mass spectrometry on a Thermo Fisher LTQ Orbitrap Velos Pro mass spectrometer. The Xcalibur raw files were converted to mzXML format and were searched against the UniProtKB/Swiss-Prot human protein database (UniProt release 2016_04) using X! TANDEM CYCLONE TPP (2011.12.01.1 - LabKey, Insilicos, ISB). Methionine oxidation was considered as a variable modification in all searches. For biotinylated cell surface proteins, EZ-LINK biotinylation of N-terminus and lysine were considered as variable modifications. Up to one missed tryptic cleavage was allowed. The X! Tandem search results were analyzed by the Trans-Proteomic Pipeline, version 4.3. Peptide/protein identifications were validated by the Peptide/ProteinProphet software tools.[46,47] A ProteinProphet score of 0.9 was used as a cutoff, which corresponded to false discovery rates of 0.7%, 0.7%, 0.9%, and 0.8% in the Y79 secretome, RB383 secretome, Y79 surface proteome, and RB383 surface proteome datasets, respectively.

RNA samples, real-time quantitative RT-PCR, and RNA sequencing—De-identified retinoblastoma tumor RNA samples were obtained from the Cooperative Human Tissue Network. Total cellular RNA was isolated using TRIzol reagent (Invitrogen). Reverse transcription was performed using High Capacity cDNA Reverse Transcription Kit (Thermo Fisher) as per manufacturer's instructions. Quantitative PCR was performed using PowerUp SYBR Green Master Mix (Thermo Fisher) on Applied Biosystems ViiA 7 Real-Time PCR System. Each sample was analyzed in triplicate. The following primers were used: SFRP2 forward 5′-TTGAGTGCGACCGTTTCC-3′, SFRP2 reverse 5′-AAGCGTTTCCATTATGTCGTTG-3′, CXADR forward 5′-CTGTGCGGAGTAGTGGATTT-3′, CXADR reverse 5′-GTCTTCGGGACTAAGCGTAAA-3′, NOS2 forward 5′-GGAGACCCAAGA GAAGAGAGA-3′, NOS2 reverse 5′-CAAAGAGGATGGTGACTCTGAC-3′, NOS3 forward 5′-CATCACCAGGAAGAAGACCTTTA-3′, NOS3 reverse 5′-TACAGGATTGTCGCCTTCAC-3′, GAPDH forward, 5′-GGTGTGAACCATGAGAAGTATGA-3′, and GAPDH reverse, 5′-GAGTCCTTCCACGATACCAAAG-3′. RNA-sequencing was performed as described.[26] Briefly, cDNA fragment libraries were synthesized using TruSeq stranded mRNA library preparation kit (Illumina). Samples were sequenced on the Illumina HiSeq 3000 platform (Illumina Inc.) using a 50 base-pair single-read (50SR) sequencing module. Sequence reads were aligned to hg19 genome build using TopHat2 with default parameters and quantified with HTSeq algorithm. Differential expression analysis was performed using DESeq (at least 2 fold changes with p value <0.05), followed by functional assessment using Database for Annotation, Visualization and Integrated Discovery (DAVID, http://david.abcc.ncifcrf.gov/)[48] and Ingenuity Pathway Analysis (IPA, Ingenuity Systems, http://www.ingenuity.com). The RNA sequencing data were deposited in the GEO database (the accession number: GSE161990).

Immunoblotting, immunoprecipitation, and immunohistochemistry—Fifteen micrograms of whole-cell lysate or 20 μg of conditioned medium was separated by SDS-PAGE and analyzed by immunoblotting as described.[49] For immunoprecipitation, cells were lysed in TNE buffer (10 mM Tris [pH 7.4], 150 mM NaCl, 1% Nonidet P-40, 1 mM EDTA, and protease inhibitors) as described.[50] Immunohistochemistry was performed as described.[51] The following antibodies were used: SFRP2 (MBS855517, MyBioSource; for immunoblotting); SFRP2 (MABC539, Millipore; for immunohistochemistry); PARP (9542, Cell Signaling Technology); tubulin (Developmental Studies Hybridoma Bank); nNOS/NOS1 (4231, Cell Signaling Technology); iNOS/NOS2 (3120, Cell Signaling Technology); eNOS/NOS3 (32,027, Cell Signaling Technology); p21 (2946, Cell Signaling Technology); p53 (sc-126, Santa Cruz Biotechnology); phospho-CREB (Ser133, 9198, Cell Signaling Technology); CXADR (A302-847A, Bethyl Laboratories); FLAG (F1804, Sigma-Aldrich); and β-catenin (9582, Cell Signaling Technology).

Cell proliferation and xenograft tumorigenicity assays—Cell proliferation was assessed by the IncuCyte live-cell imaging system (Essen BioScience). For subcutaneous xenograft tumorigenicity assays, retinoblastoma cells were subcutaneously injected into the flanks of SCID mice (1×10^6 cells/injection, five mice/group). Tumor growth was monitored weekly using a caliper. For orthotopic xenograft tumorigenicity assays, retinoblastoma cells engineered to express luciferase were injected into the right vitreous bodies of SCID mice (5×10^4 cells/injection, three mice/group) and tumor growth was monitored by Xenogen IVIS imaging system. Mice were randomly allocated to treatment groups. Blinding of the researcher measuring tumor size was employed. The animal research method was reviewed and approved for humaneness by the Institutional Animal Care and Use Committee.

Microscale thermophoresis—Recombinant human CXADR protein (3336-CX-050, R&D Systems) was labeled using the protein labeling kit (RED-NHS second generation, MO-L011, Nano Temper Technologies) according to the manufacturer's protocol. Recombinant human SFRP2 protein (6838-FR-025, R&D Systems) was combined with labeled CXADR protein in PBS/0.005% Tween 20. After 30-min incubation at room temperature, the samples were loaded to the capillary chips of the Monolith NT.115 instrument (NanoTemper Technologies). The data analysis was performed using MO Affinity Analysis Software (NanoTemper Technologies).

Phage display library screening—The Ph.D.-12 Phage Display Peptide Library (New England Biolabs) was screened with recombinant human SFRP2 protein (6838-FR-025, R&D Systems) following the New England Biolabs' protocol. After three cycles of binding, washing, and phage amplification, the phage inserts encoding the 12-mer peptides were sequenced. The SFRP2-binding peptides were synthesized by GenScript Biotech.

QUANTIFICATION AND STATISTICAL ANALYSIS

Statistical analysis—Data are expressed as mean ± SEM. Two-tailed Student's t tests were used to calculate the p values except for Figure 1H in which exact Wilcoxon – Mann – Whitney test[29] was used. The results were considered significant when $p < 0.05$. The number of replicates, independent samples, and animals is indicated in the figure legends.

Supplementary Material

Refer to Web version on PubMed Central for supplementary material.

ACKNOWLEDGMENTS

We thank Robert Eisenman for helpful discussions and critical review of the manuscript. We thank Anna Falk for AF22 cells, the Cooperative Human Tissue Network for retinoblastoma tumor RNA samples, and the University of Texas Health Science Center at San Antonio (UTHSCSA) Institutional Mass Spectrometry Laboratory (Sammy Pardo and Dana Molleur) for mass spectrometry analysis. This work was supported by the National Cancer Institute, National Institutes of Health (CA202485 to Y.S. and CA165995 to P.J.H.); by the Cancer Prevention and Research Institute of Texas (RP160487, RP160841, and RP190385 to Y.S.; RP160716 to P.J.H.; RP160732 to Y.C.); by the Owens Medical Research Foundation (to Y.S.); by the National Center for Advancing Translational Sciences, National Institutes of Health, through the Clinical and Translational Science Award (CTSA) UL1 TR001120; by the Mays Cancer Center P30 Cancer Center Support Grant from the National Cancer Institute (CA054174) for the mass spectrometry, flow cytometry, and next-generation sequencing shared resources; by the National Institutes of Health for purchase of the Orbitrap mass spectrometer (1S10RR025111-01 to S.T.W.) and the HiSeq 3000 sequencer (1S10OD021805-01); and by the Greehey Children's Cancer Research Institute Pilot Project Award (to Y.S.).

REFERENCES

1. Furchgott RF, and Zawadzki JV (1980). The obligatory role of endothelial cells in the relaxation of arterial smooth muscle by acetylcholine. Nature 288, 373–376. 10.1038/288373a0. [PubMed: 6253831]
2. McDonald LJ, and Murad F (1995). Nitric oxide and cGMP signaling. Adv. Pharmacol. 34, 263–275. 10.1016/s1054-3589(08)61091-1. [PubMed: 8562439]
3. Ignarro LJ, Buga GM, Wood KS, Byrns RE, and Chaudhuri G (1987). Endothelium-derived relaxing factor produced and released from artery and vein is nitric oxide. Proc. Natl. Acad. Sci. USA 84, 9265–9269. 10.1073/pnas.84.24.9265. [PubMed: 2827174]
4. Martínez-Ruiz A, Cadenas S, and Lamas S (2011). Nitric oxide signaling: classical, less classical, and nonclassical mechanisms. Free Radic. Biol. Med. 51, 17–29. 10.1016/j.freeradbiomed.2011.04.010. [PubMed: 21549190]
5. Dimaras H, Corson TW, Cobrinik D, White A, Zhao J, Munier FL, Abramson DH, Shields CL, Chantada GL, Njuguna F, and Gallie BL (2015). Retinoblastoma. Nat. Rev. Dis. Prim. 1, 15021. 10.1038/nrdp.2015.21. [PubMed: 27189421]
6. Benavente CA, and Dyer MA (2015). Genetics and epigenetics of human retinoblastoma. Annu. Rev. Pathol. 10, 547–562. 10.1146/annurev-pathol-012414-040259. [PubMed: 25621664]
7. Zhang J, Benavente CA, McEvoy J, Flores-Otero J, Ding L, Chen X, Ulyanov A, Wu G, Wilson M, Wang J, et al. (2012). A novel retinoblastoma therapy from genomic and epigenetic analyses. Nature 481, 329–334. 10.1038/nature10733. [PubMed: 22237022]
8. Kooi IE, Mol BM, Massink MPG, Ameziane N, Meijers-Heijboer H, Dommering CJ, van Mil SE, de Vries Y, van der Hout AH, Kaspers GJL, et al. (2016). Somatic genomic alterations in retinoblastoma beyond RB1 are rare and limited to copy number changes. Sci. Rep. 6, 25264. 10.1038/srep25264. [PubMed: 27126562]
9. Robanus-Maandag E, Dekker M, van der Valk M, Carrozza ML, Jeanny JC, Dannenberg JH, Berns A, and te Riele H (1998). p107 is a suppressor of retinoblastoma development in pRb-deficient mice. Genes Dev. 12, 1599–1609. 10.1101/gad.12.11.1599. [PubMed: 9620848]
10. Chen D, Livne-bar I, Vanderluit JL, Slack RS, Agochiya M, and Bremner R (2004). Cell-specific effects of RB or RB/p107 loss on retinal development implicate an intrinsically death-resistant cell-of-origin in retinoblastoma. Cancer Cell 5, 539–551. 10.1016/j.ccr.2004.05.025. [PubMed: 15193257]
11. MacPherson D, Sage J, Kim T, Ho D, McLaughlin ME, and Jacks T (2004). Cell type-specific effects of Rb deletion in the murine retina. Genes Dev. 18, 1681–1694. 10.1101/gad.1203304. [PubMed: 15231717]

12. Dannenberg JH, Schuijff L, Dekker M, van der Valk M, and te Riele H (2004). Tissue-specific tumor suppressor activity of retinoblastoma gene homologs p107 and p130. Genes Dev. 18, 2952–2962. 10.1101/gad.322004. [PubMed: 15574596]

13. Zhang J, Schweers B, and Dyer MA (2004). The first knockout mouse model of retinoblastoma. Cell Cycle 3, 952–959. [PubMed: 15190215]

14. Sangwan M, McCurdy SR, Livne-Bar I, Ahmad M, Wrana JL, Chen D, and Bremner R (2012). Established and new mouse models reveal E2f1 and Cdk2 dependency of retinoblastoma, and expose effective strategies to block tumor initiation. Oncogene 31, 5019–5028. 10.1038/onc.2011.654. [PubMed: 22286767]

15. Dyer MA, and Bremner R (2005). The search for the retinoblastoma cell of origin. Nat. Rev. Cancer 5, 91–101. 10.1038/nrc1545. [PubMed: 15685194]

16. Xu XL, Fang Y, Lee TC, Forrest D, Gregory-Evans C, Almeida D, Liu A, Jhanwar SC, Abramson DH, and Cobrinik D (2009). Retinoblastoma has properties of a cone precursor tumor and depends upon cone-specific MDM2 signaling. Cell 137, 1018–1031. 10.1016/j.cell.2009.03.051. [PubMed: 19524506]

17. Xu XL, Singh HP, Wang L, Qi DL, Poulos BK, Abramson DH, Jhanwar SC, and Cobrinik D (2014). Rb suppresses human cone-precursor-derived retinoblastoma tumours. Nature 514, 385–388. 10.1038/nature13813. [PubMed: 25252974]

18. Esteve P, Sandonìs A, Cardozo M, Malapeira J, Ibañez C, Crespo I, Marcos S, Gonzalez-Garcia S, Toribio ML, Arribas J, et al. (2011). SFRPs act as negative modulators of ADAM10 to regulate retinal neurogenesis. Nat. Neurosci. 14, 562–569. 10.1038/nn.2794. [PubMed: 21478884]

19. Herrera E, Erskine L, and Morenilla-Palao C (2019). Guidance of retinal axons in mammals. Semin. Cell Dev. Biol. 85, 48–59. 10.1016/j.semcdb.2017.11.027. [PubMed: 29174916]

20. Marcos S, Nieto-Lopez F, Sandonìs A, Cardozo MJ, Di Marco F, Esteve P, and Bovolenta P (2015). Secreted frizzled related proteins modulate pathfinding and fasciculation of mouse retina ganglion cell axons by direct and indirect mechanisms. J. Neurosci. 35, 4729–4740. 10.1523/JNEUROSCI.3304-13.2015. [PubMed: 25788689]

21. Kawano Y, and Kypta R (2003). Secreted antagonists of the Wnt signalling pathway. J. Cell Sci. 116, 2627–2634. [PubMed: 12775774]

22. Suzuki H, Gabrielson E, Chen W, Anbazhagan R, van Engeland M, Weijenberg MP, Herman JG, and Baylin SB (2002). A genomic screen for genes upregulated by demethylation and histone deacetylase inhibition in human colorectal cancer. Nat. Genet. 31, 141–149. [PubMed: 11992124]

23. Surana R, Sikka S, Cai W, Shin EM, Warrier SR, Tan HJG, Arfuso F, Fox SA, Dharmarajan AM, and Kumar AP (2014). Secreted frizzled related proteins: implications in cancers. Biochim. Biophys. Acta 1845, 53–65. 10.1016/j.bbcan.2013.11.004. [PubMed: 24316024]

24. Liu Y, Zhou Q, Zhou D, Huang C, Meng X, and Li J (2017). Secreted frizzled-related protein 2-mediated cancer events: friend or foe? Pharmacol. Rep. 69, 403–408. 10.1016/j.pharep.2017.01.001. [PubMed: 28273499]

25. Kaur A, Webster MR, Marchbank K, Behera R, Ndoye A, Kugel CH 3rd, Dang VM, Appleton J, O'Connell MP, Cheng P, et al. (2016). sFRP2 in the aged microenvironment drives melanoma metastasis and therapy resistance. Nature 532, 250–254. 10.1038/nature17392. [PubMed: 27042933]

26. Elzi DJ, Song M, Blackman B, Weintraub ST, López-Terrada D, Chen Y, Tomlinson GE, and Shiio Y (2016). FGF19 functions as autocrine growth factor for hepatoblastoma. Genes Cancer 7, 125–135. 10.18632/genesandcancer.101. [PubMed: 27382436]

27. Zhou F, Elzi DJ, Jayabal P, Ma X, Chiu YC, Chen Y, Blackman B, Weintraub ST, Houghton PJ, and Shiio Y (2020). GDF6-CD99 signaling regulates src and ewing sarcoma growth. Cell Rep. 33, 108332. 10.1016/j.celrep.2020.108332. [PubMed: 33147457]

28. Hudson LE, Mendoza P, Hudson WH, Ziesel A, Hubbard GB 3rd, Wells J, Dwivedi B, Kowalski J, Seby S, Patel V, et al. (2018). Distinct gene expression profiles define anaplastic grade in retinoblastoma. Am. J. Pathol. 188, 2328–2338. 10.1016/j.ajpath.2018.06.013. [PubMed: 30036517]

29. Marx A, Backes C, Meese E, Lenhof HP, and Keller A (2016). EDISON-WMW: exact dynamic programing solution of the wilcoxon-mann-whitney test. Dev. Reprod. Biol. 14, 55–61. 10.1016/j.gpb.2015.11.004.
30. Haik BG, Dunleavy SA, Cooke C, Ellsworth RM, Abramson DH, Smith ME, and Karcioglu ZA (1987). Retinoblastoma with anterior chamber extension. Ophthalmology 94, 367–370. 10.1016/s0161-6420(87)33437-2. [PubMed: 3587918]
31. Shields CL, Shields JA, Baez KA, Cater J, and De Potter PV (1993). Choroidal invasion of retinoblastoma: metastatic potential and clinical risk factors. Br. J. Ophthalmol. 77, 544–548. 10.1136/bjo.77.9.544. [PubMed: 8218048]
32. Shields CL, Shields JA, Baez K, Cater JR, and De Potter P (1994). Optic nerve invasion of retinoblastoma. Metastatic potential and clinical risk factors. Cancer 73, 692–698. 10.1002/1097-0142(19940201)73:3<692::aid-cncr2820730331>3.0.co;2-8. [PubMed: 8299091]
33. Falk A, Koch P, Kesavan J, Takashima Y, Ladewig J, Alexander M, Wiskow O, Tailor J, Trotter M, Pollard S, et al. (2012). Capture of neuroepithelial-like stem cells from pluripotent stem cells provides a versatile system for in vitro production of human neurons. PLoS One 7, e29597. 10.1371/journal.pone.0029597. [PubMed: 22272239]
34. Hwang TL, Tang MC, Kuo LM, Chang WD, Chung PJ, Chang YW, and Fang YC (2012). YC-1 potentiates cAMP-induced CREB activation and nitric oxide production in alveolar macrophages. Toxicol. Appl. Pharmacol. 260, 193–200. 10.1016/j.taap.2012.02.011. [PubMed: 22381622]
35. Imai T, Hirata Y, Kanno K, and Marumo F (1994). Induction of nitric oxide synthase by cyclic AMP in rat vascular smooth muscle cells. J. Clin. Invest. 93, 543–549. 10.1172/JCI117005. [PubMed: 7509342]
36. Kunz D, Mühl H, Walker G, and Pfeilschifter J (1994). Two distinct signaling pathways trigger the expression of inducible nitric oxide synthase in rat renal mesangial cells. Proc. Natl. Acad. Sci. USA 91, 5387–5391. 10.1073/pnas.91.12.5387. [PubMed: 7515501]
37. Matthäus C, Langhorst H, Schütz L, Jüttner R, and Rathjen FG (2017). Cell-cell communication mediated by the CAR subgroup of immunoglobulin cell adhesion molecules in health and disease. Mol. Cell. Neurosci. 81, 32–40. 10.1016/j.mcn.2016.11.009. [PubMed: 27871939]
38. Ortiz-Zapater E, Santis G, and Parsons M (2017). CAR: a key regulator of adhesion and inflammation. Int. J. Biochem. Cell Biol. 89, 1–5. 10.1016/j.biocel.2017.05.025. [PubMed: 28545889]
39. Pascual-Pasto G, Bazan-Peregrino M, Olaciregui NG, Restrepo-Perdomo CA, Mato-Berciano A, Ottaviani D, Weber K, Correa G, Paco S, Vila-Ubach M, et al. (2019). Therapeutic targeting of the RB1 pathway in retinoblastoma with the oncolytic adenovirus VCN-01. Sci. Transl. Med. 11, eaat9321. 10.1126/scitranslmed.aat9321. [PubMed: 30674657]
40. Go CD, Knight JDR, Rajasekharan A, Rathod B, Hesketh GG, Abe KT, Youn JY, Samavarchi-Tehrani P, Zhang H, Zhu LY, et al. (2021). A proximity-dependent biotinylation map of a human cell. Nature 595, 120–124. 10.1038/s41586-021-03592-2. [PubMed: 34079125]
41. Bodine PVN, Stauffer B, Ponce-de-Leon H, Bhat RA, Mangine A, Seestaller-Wehr LM, Moran RA, Billiard J, Fukayama S, Komm BS, et al. (2009). A small molecule inhibitor of the Wnt antagonist secreted frizzled-related protein-1 stimulates bone formation. Bone 44, 1063–1068. 10.1016/j.bone.2009.02.013. [PubMed: 19254787]
42. Bergelson JM, Cunningham JA, Droguett G, Kurt-Jones EA, Krithivas A, Hong JS, Horwitz MS, Crowell RL, and Finberg RW (1997). Isolation of a common receptor for Coxsackie B viruses and adenoviruses 2 and 5. Science 275, 1320–1323. 10.1126/science.275.5304.1320. [PubMed: 9036860]
43. Tomko RP, Xu R, and Philipson L (1997). HCAR and MCAR: the human and mouse cellular receptors for subgroup C adenoviruses and group B coxsackieviruses. Proc. Natl. Acad. Sci. USA 94, 3352–3356. 10.1073/pnas.94.7.3352. [PubMed: 9096397]
44. Jayabal P, Houghton PJ, and Shiio Y (2017). EWS-FLI-1 creates a cell surface microenvironment conducive to IGF signaling by inducing pappalysin-1. Genes Cancer 8, 762–770. 10.18632/genesand-cancer.159. [PubMed: 29321818]

45. Özlü N, Qureshi MH, Toyoda Y, Renard BY, Mollaoglu G, Özkan NE, Bulbul S, Poser I, Timm W, Hyman AA, et al. (2015). Quantitative comparison of a human cancer cell surface proteome between interphase and mitosis. EMBO J. 34, 251–265. 10.15252/embj.201385162. [PubMed: 25476450]

46. Keller A, Nesvizhskii AI, Kolker E, and Aebersold R (2002). Empirical statistical model to estimate the accuracy of peptide identifications made by MS/MS and database search. Anal. Chem. 74, 5383–5392. [PubMed: 12403597]

47. Nesvizhskii AI, Keller A, Kolker E, and Aebersold R (2003). A statistical model for identifying proteins by tandem mass spectrometry. Anal. Chem. 75, 4646–4658. [PubMed: 14632076]

48. Huang DW, Sherman BT, and Lempicki RA (2009). Systematic and integrative analysis of large gene lists using DAVID bioinformatics resources. Nat. Protoc. 4, 44–57. 10.1038/nprot.2008.211. [PubMed: 19131956]

49. Jayabal P, Zhou F, Lei X, Ma X, Blackman B, Weintraub ST, Houghton PJ, and Shiio Y (2021). NELL2-cdc42 signaling regulates BAF complexes and Ewing sarcoma cell growth. Cell Rep. 36, 109254. 10.1016/j.celrep.2021.109254. [PubMed: 34233189]

50. Shiio Y, and Eisenman RN (2003). Histone sumoylation is associated with transcriptional repression. Proc. Natl. Acad. Sci. USA 100, 13225–13230. [PubMed: 14578449]

51. Elzi DJ, Lai Y, Song M, Hakala K, Weintraub ST, and Shiio Y (2012). Plasminogen activator inhibitor 1--insulin-like growth factor binding protein 3 cascade regulates stress-induced senescence. Proc. Natl. Acad. Sci. USA 109, 12052–12057. [PubMed: 22778398]

Highlights

- The autocrine signaling mediated by SFRP2 drives retinoblastoma
- SFRP2 signaling suppresses NO production and maintains retinoblastoma growth
- CXADR serves as the receptor for SFRP2
- Targeting SFRP2 results in NO production and suppression of retinoblastoma growth

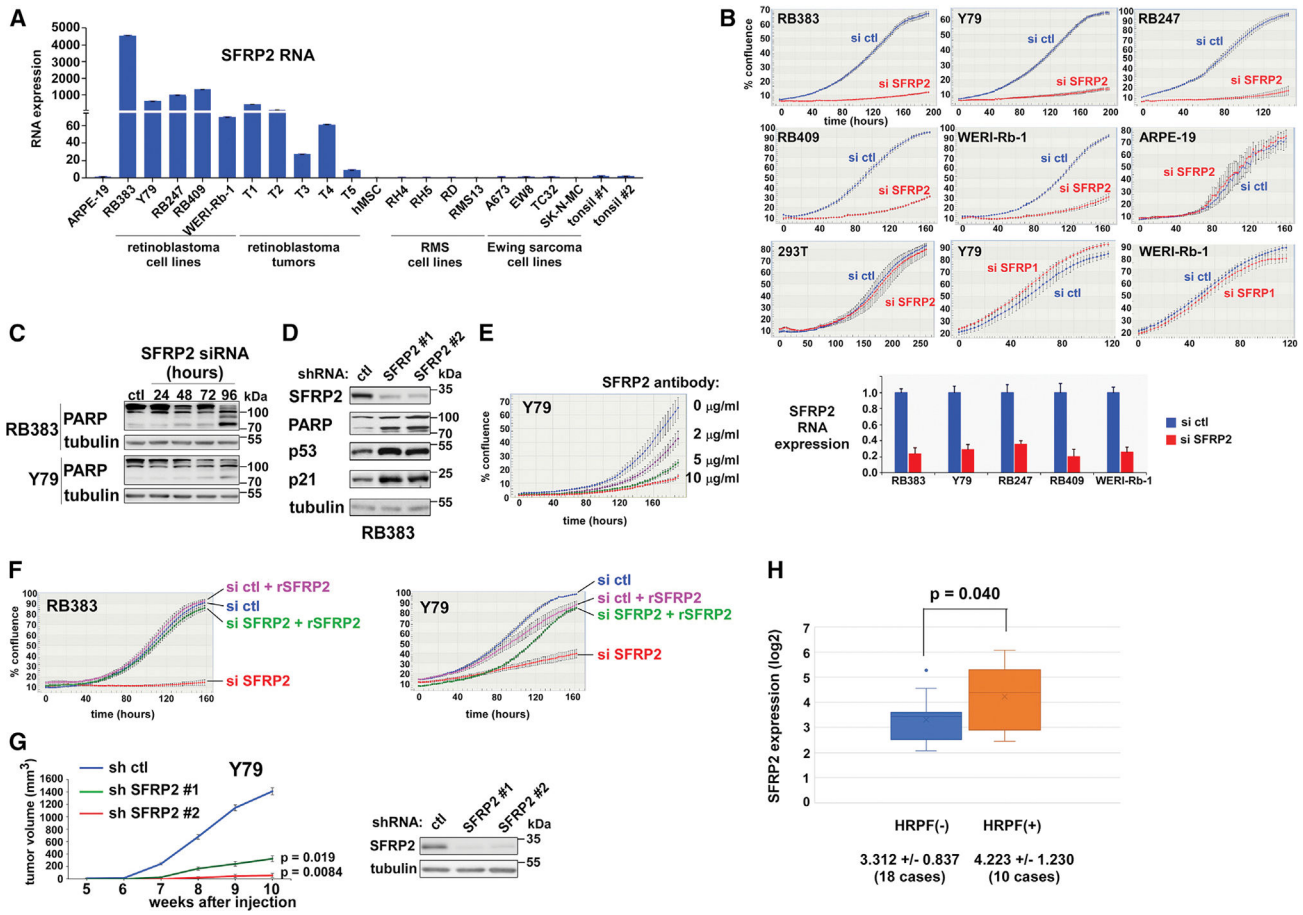

Figure 1. Retinoblastoma depends on SFRP2

(A) SFRP2 is highly expressed in retinoblastoma tumors and cell lines. SFRP2 RNA expression was analyzed by quantitative real-time RT-PCR (qRT-PCR) and was normalized to the levels in human ARPE-19 retinal pigment epithelial cells (n = 3). All data in bar graphs are expressed as mean ± SEM.

(B) SFRP2 silencing inhibits retinoblastoma proliferation. SFRP2 was silenced by siRNA transfection in retinoblastoma cells (RB383, Y79, RB247, RB409, WERI-Rb-1) and control cells (ARPE-19 retinal pigment epithelial cells and 293T embryonic kidney cells), and cell proliferation was assessed by the IncuCyte live-cell imaging system (top). SFRP2 silencing inhibited the proliferation of retinoblastoma cells but not control cells. Additionally, SFRP1 siRNA transfection did not affect the proliferation of Y79 and WERI-Rb-1 cells. SFRP2 silencing was verified by qRT-PCR (bottom; RNA expression normalized to GAPDH, n = 3).

(C) SFRP2 siRNA silencing induces apoptosis in retinoblastoma cells. RB383 and Y79 cells were transfected with SFRP2 siRNA, and the induction of apoptosis was assessed by the cleavage of PARP. Tubulin served as a loading control.

(D) SFRP2 shRNA silencing induces apoptosis in retinoblastoma cells. RB383 cells were infected with lentiviruses expressing SFRP2 shRNA or control shRNA, and the induction of apoptosis was assessed by the cleavage of PARP.

(E) An anti-SFRP2 antibody inhibits retinoblastoma proliferation. An anti-SFRP2 rabbit polyclonal antibody (sc-13940, Santa Cruz Biotechnology) was added at the indicated concentration to Y79 cells, and cell proliferation was assessed by IncuCyte.

(F) Recombinant SFRP2 rescues proliferation inhibition of retinoblastoma cells following SFRP2 silencing. RB383 and Y79 cells were transfected with SFRP2 siRNA or control siRNA and were treated with and without recombinant SFRP2 (6838-FR-025, R&D Systems; used at 250 ng/mL). Cell proliferation was assessed by IncuCyte.

(G) SFRP2 silencing inhibits xenograft tumorigenicity of Y79 cells. SFRP2 was silenced by lentiviral expression of two different shRNAs (right), and xenograft tumor growth was assessed by subcutaneous injection in SCID mice (left). SFRP2 silencing profoundly inhibited xenograft tumor growth. Data are expressed as mean ± SEM; p values were calculated using Student's t test (two tailed); n = 5.

(H) Retinoblastoma tumors with high-risk pathologic features (HRPFs) display higher SFRP2 expression than those without HRPFs. The retinoblastoma tumor RNA expression data in Hudson et al.[28] were used. Tumors with HRPFs, 10 cases; tumors without HRPFs, 18 cases. p = 0.040 using exact Wilcoxon-Mann-Whitney test.[29]

A

Name	p-value
iNOS Signaling	2.38E-04
PI3K Signaling in B Lymphocytes	2.54E-04
MIF Regulation of Innate Immunity	3.04E-03
Sumoylation Pathway	4.08E-03
Cholecystokinin/Gastrin-mediated Signaling	4.88E-03
RANK Signaling in Osteoclasts	5.01E-03
Role of Macrophages, in Rheumatoid Arthritis	5.37E-03
T Cell Receptor Signaling	6.46E-03
L-cysteine Degradation II	6.76E-03
Corticotropin Releasing Hormone Signaling	7.24E-03
Granzyme A Signaling	7.94E-03
Production of Nitric Oxide and Reactive Oxygen Species in Macrophages	1.02E-02

B

Name	activation z-score	p-value
CREB1	2.032	3.12E-10
ethanol	1.424	2.87E-07
GnRH-A	2.040	6.21E-07
CD24		7.89E-07
MEF2C		9.73E-07

C

Name	activation z-score	p-value
p53	5.706	1.45E-14
CDKN1A	1.813	2.11E-13
ESR1	-3.376	4.19E-12
HGF	-1.746	1.87E-10
ERBB2	1.017	4.91E-10

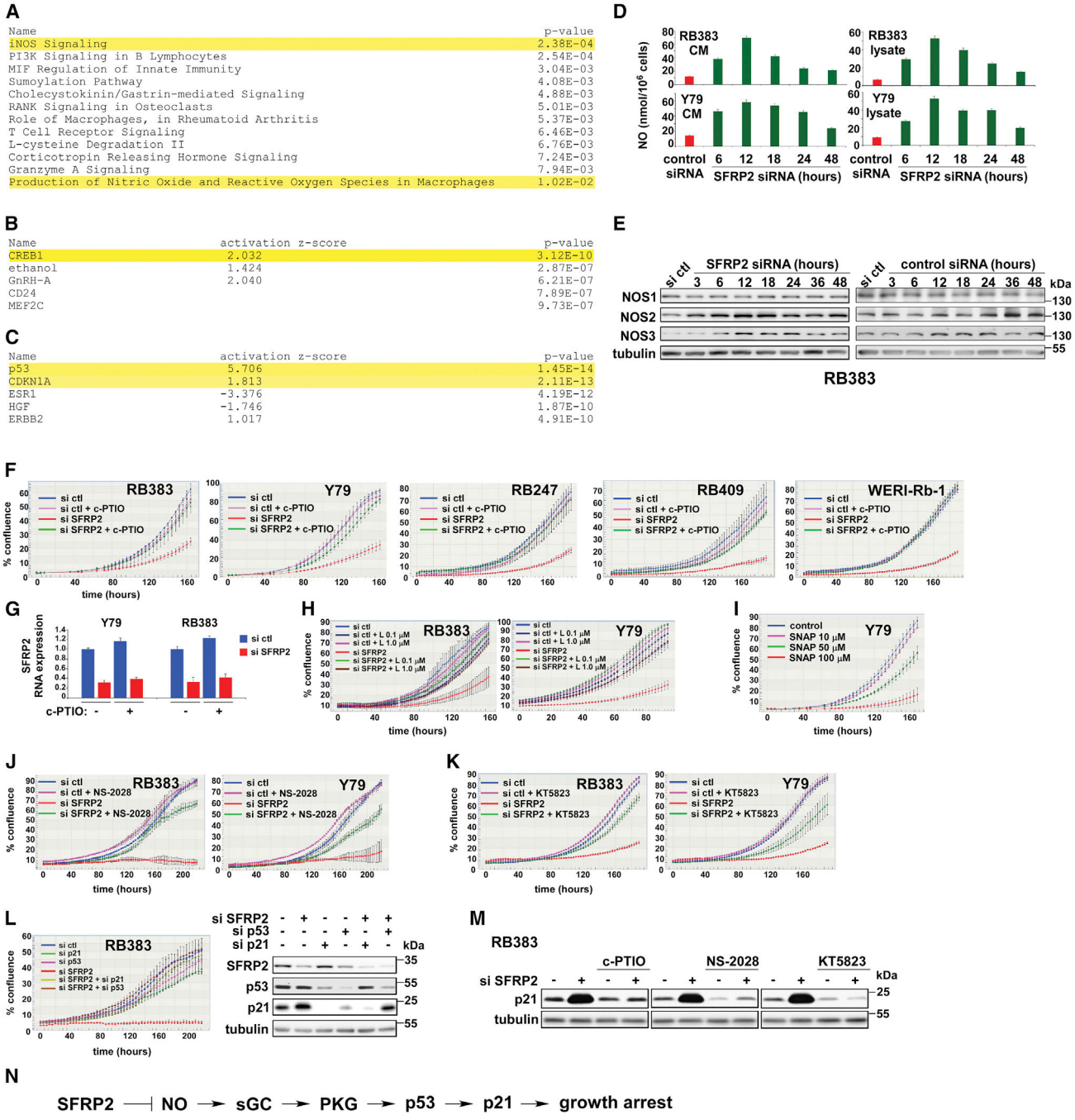

Figure 2. NO mediates growth inhibition following SFRP2 silencing

(A) The top canonical pathways identified by Ingenuity Pathway Analysis of gene expression changes in SFRP2-silenced RB383 cells at 24 h.

(B) The top upstream regulators identified by Ingenuity Pathway Analysis of gene expression changes in SFRP2-silenced RB383 cells at 24 h.

(C) The top upstream regulators identified by Ingenuity Pathway Analysis of gene expression changes in SFRP2-silenced RB383 cells at 48 h.

(D) SFRP2 silencing results in rapid production of NO in retinoblastoma. RB383 and Y79 cells were transfected with SFRP2 siRNA, and the production of NO was assessed by nitrite/nitrate calorimetric assays of the conditioned medium (CM) and cell lysate (n = 3).
(E) SFRP2 silencing results in rapid induction of NOS2 (iNOS) and NOS3 (eNOS). RB383 cells were transfected with SFRP2 siRNA or control siRNA, and the levels of indicated proteins were examined by immunoblotting. Tubulin served as a loading control. A representative result from three independent experiments is shown.
(F) Growth inhibition following SFRP2 silencing can be rescued by a NO scavenger, carboxy-PTIO. Retinoblastoma cells were transfected with SFRP2 siRNA or control siRNA and were treated with 1 μM carboxy-PTIO or left untreated. Cell proliferation was assessed by IncuCyte.
(G) Carboxy-PTIO treatment does not affect SFRP2 silencing in retinoblastoma (n = 3).
(H) Growth inhibition following SFRP2 silencing can be rescued by a pan-NOS inhibitor, L-NMMA. Retinoblastoma cells were transfected with SFRP2 siRNA or control siRNA and were treated with the indicated concentration of L-NMMA (L). Cell proliferation was assessed by IncuCyte.
(I) An NO donor, SNAP, inhibits retinoblastoma proliferation in a dose-dependent fashion. Y79 cells were treated with the indicate concentration of SNAP, and cell proliferation was assessed by IncuCyte.
(J) Growth inhibition following SFRP2 silencing can be rescued by an sGC inhibitor, NS-2028. Retinoblastoma cells were transfected with SFRP2 siRNA or control siRNA and treated with 5 μM NS-2028 or left untreated. Cell proliferation was assessed by IncuCyte.
(K) Growth inhibition following SFRP2 silencing can be rescued by a protein kinase G inhibitor, KT5823. Retinoblastoma cells were transfected with SFRP2 siRNA or control siRNA and treated with 2.5 μM KT5823 or left untreated. Cell proliferation was assessed by IncuCyte.
(L) Growth inhibition following SFRP2 silencing can be rescued by simultaneous silencing of p53 or p21. RB383 cells were transfected with SFRP2 siRNA, p53 siRNA, p21 siRNA, and/or control siRNA as indicated. Cell proliferation was assessed by IncuCyte (left). The silencing of SFRP2, p53, and p21 was verified by immunoblotting (right).
(M) p21 induction following SFRP2 silencing was abolished by carboxy-PTIO, NS-2028, and KT5823. RB383 cells were transfected with SFRP2 siRNA or control siRNA. Cells were left untreated or treated with 1 μM carboxy-PTIO, 5 μM NS-2028, or 2.5 μM KT5823 as indicated. The levels of p21 were assessed by immunoblotting.
(N) SFRP2 suppresses the production of NO in retinoblastoma. SFRP2 silencing results in production of NO, which activates soluble guanylate cyclase (sGC) and cGMP-dependent protein kinase (PKG), leading to p53-and p21-dependent growth arrest of retinoblastoma. The NO-sGC-PKG pathway is based on literature, and the roles of sGC and PKG in SFRP2 signaling are based on the effects of their pharmacological inhibitors.

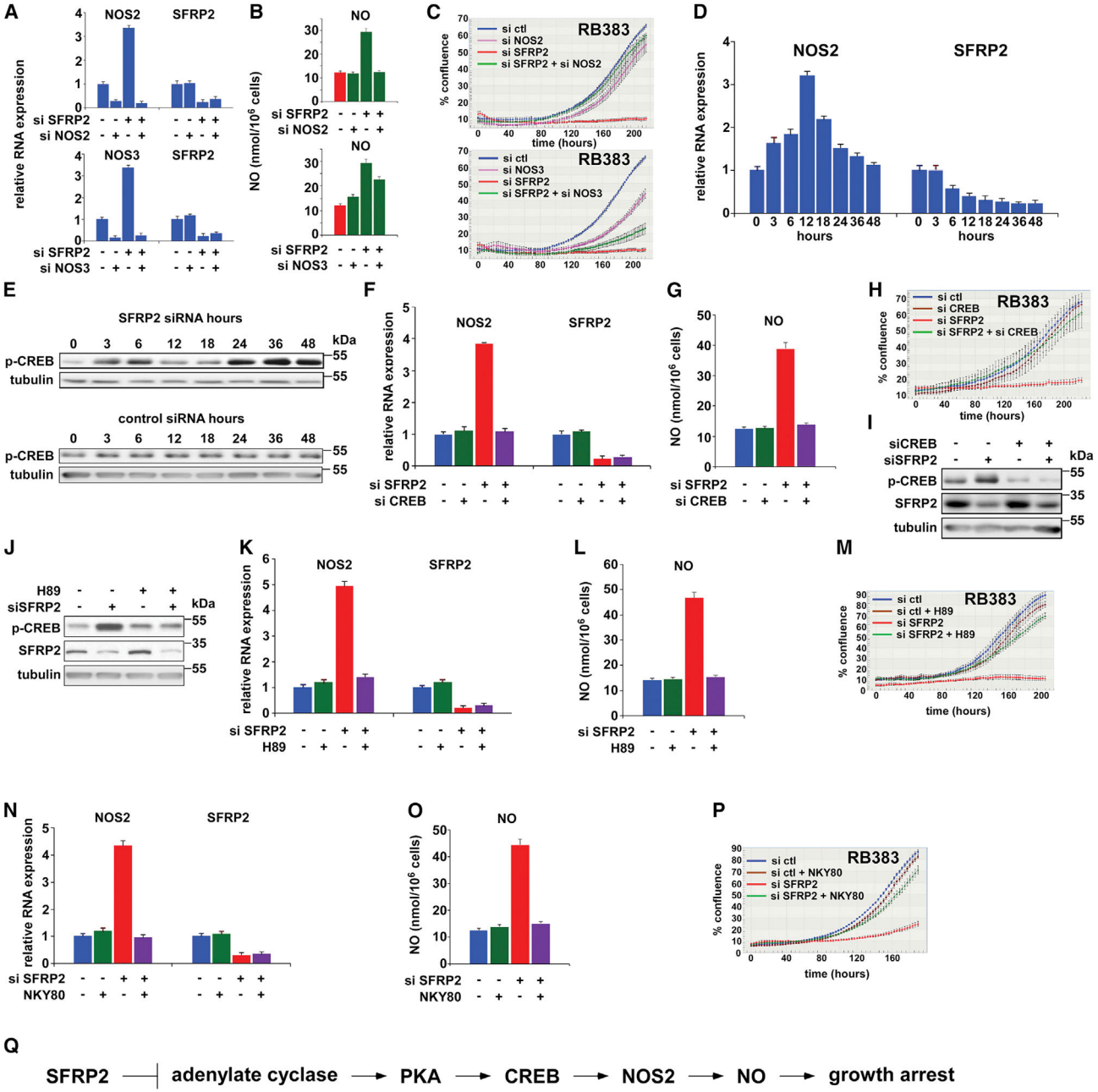

Figure 3. The adenylate cyclase-PKA-CREB-NOS2 pathway mediates NO production following SFRP2 silencing

(A) NOS2, NOS3, and SFRP2 silencing by siRNA transfection. RB383 cells were transfected with the indicated siRNAs, and the RNA levels of NOS2, NOS3, and SFRP2 were assessed by qRT-PCR 12 h after transfection (n = 3).

(B) NOS2 silencing abrogates NO production following SFRP2 silencing. RB383 cells were transfected with the indicated siRNAs, and the production of NO was assessed by nitrite/nitrate calorimetric assays of the CM 12 h after transfection (n = 3).

(C) NOS2 silencing rescues growth inhibition following SFRP2 silencing. RB383 cells were transfected with the indicated siRNAs, and cell proliferation was assessed by IncuCyte.

(D) NOS2 RNA is rapidly induced upon SFRP2 siRNA transfection. RB383 cells were transfected with SFRP2 siRNA, and the RNA levels of NOS2 and SFRP2 at the indicated time after transfection were assessed by qRT-PCR (n = 3).
(E) Phosphorylated CREB is rapidly induced upon SFRP2 siRNA transfection. RB383 cells were transfected with SFRP2 siRNA or control siRNA, and the levels of phosphorylated CREB (phospho-serine 133) were assessed by immunoblotting.
(F) CREB silencing abrogates NOS2 RNA induction following SFRP2 silencing. RB383 cells were transfected with SFRP2 siRNA, CREB siRNA, and/or control siRNA as indicated, and the RNA levels of NOS2 and SFRP2 were assessed by qRT-PCR 12 h after transfection (n = 3).
(G) CREB silencing abrogates NO production following SFRP2 silencing. RB383 cells were transfected with SFRP2 siRNA, CREB siRNA, and/or control siRNA as indicated, and the production of NO was assessed by nitrite/nitrate calorimetric assays of the CM 12 h after transfection (n = 3).
(H) CREB silencing abrogates growth inhibition following SFRP2 silencing. RB383 cells were transfected with SFRP2 siRNA, CREB siRNA, and/or control siRNA as indicated, and cell proliferation was assessed by IncuCyte.
(I) CREB and SFRP2 silencing by siRNA transfection. RB383 cells were transfected with SFRP2 siRNA, CREB siRNA, and/or control siRNA as indicated, and the protein levels of phospho-CREB and SFRP2 were assessed by immunoblotting 48 h after transfection.
(J) A PKA inhibitor, H89, abrogates CREB phosphorylation following SFRP2 silencing. RB383 cells were transfected with SFRP2 siRNA or control siRNA and treated with 5 μM H89 or left untreated, as indicated. The levels of phosphorylated CREB were assessed by immunoblotting 48 h after transfection.
(K) H89 abrogates NOS2 RNA induction following SFRP2 silencing. RB383 cells were transfected with SFRP2 siRNA or control siRNA and treated with 5 μM H89 or left untreated, as indicated. The RNA levels of NOS2 and SFRP2 were assessed by qRT-PCR 12 h after transfection (n = 3).
(L) H89 abrogates NO production following SFRP2 silencing. RB383 cells were transfected with SFRP2 siRNA or control siRNA and treated with 5 μM H89 or left untreated, as indicated. The production of NO was assessed by nitrite/nitrate calorimetric assays of the CM 12 h after transfection (n = 3).
(M) H89 abrogates growth inhibition following SFRP2 silencing. RB383 cells were transfected with SFRP2 siRNA or control siRNA and treated with 5 μM H89 or left untreated, as indicated. Cell proliferation was assessed by IncuCyte.
(N) An adenylate cyclase inhibitor, NKY80, abrogates NOS2 RNA induction following SFRP2 silencing. RB383 cells were transfected with SFRP2 siRNA or control siRNA and treated with 1 μM NKY80 or left untreated, as indicated. The RNA levels of NOS2 and SFRP2 were assessed by qRT-PCR 12 h after transfection (n = 3).
(O) NKY80 abrogates NO production following SFRP2 silencing. RB383 cells were transfected with SFRP2 siRNA or control siRNA and treated with 1 μM NKY80 or left untreated, as indicated. The production of NO was assessed by nitrite/nitrate calorimetric assays of the CM 12 h after transfection (n = 3).

(P) NKY80 abrogates growth inhibition following SFRP2 silencing. RB383 cells were transfected with SFRP2 siRNA or control siRNA and treated with 1 μM NKY80 or left untreated, as indicated. Cell proliferation was assessed by IncuCyte.
(Q) SFRP2 silencing results in NO production through the adenylate cyclase-PKA-CREB-NOS2 pathway.

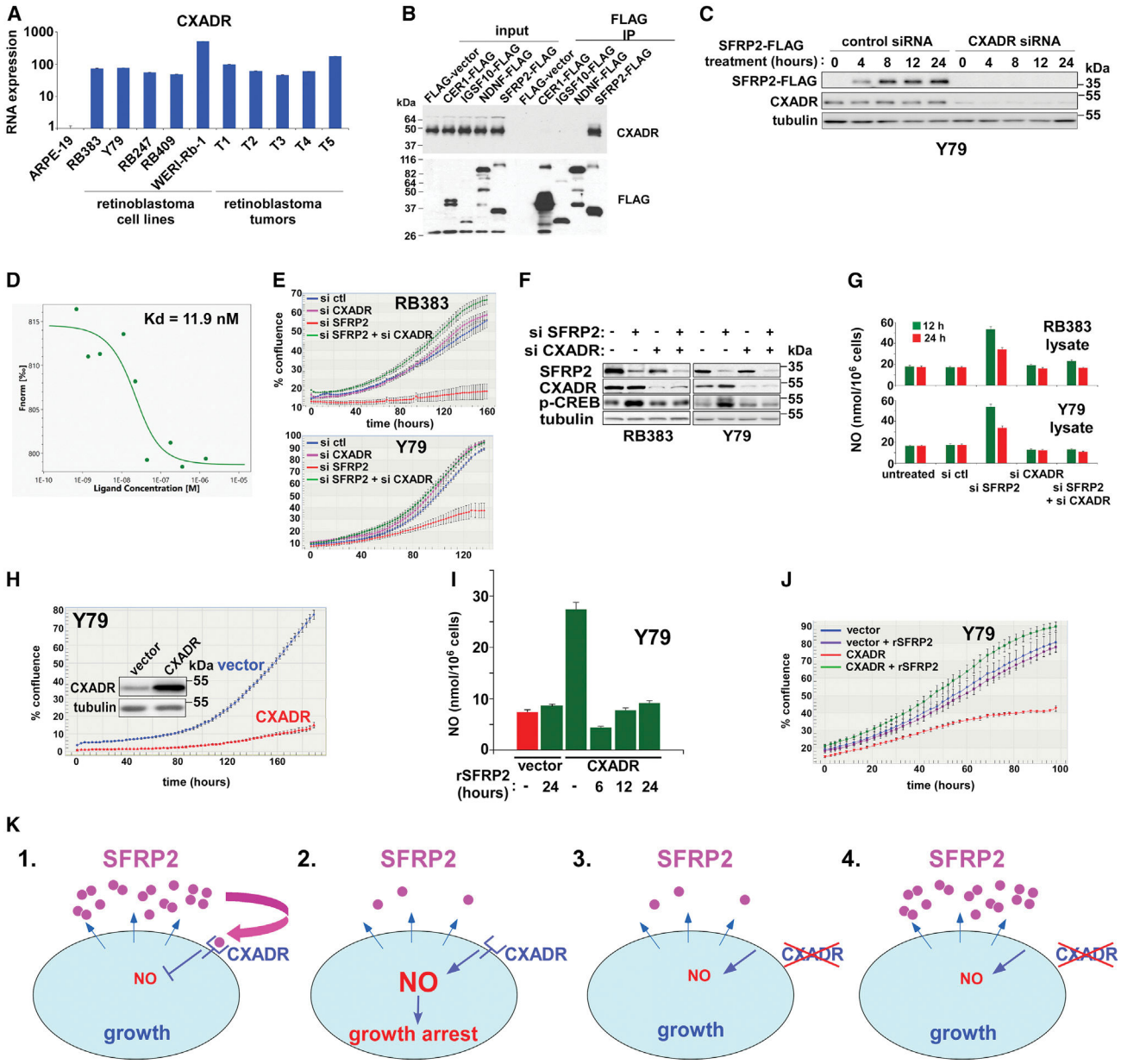

Figure 4. CXADR serves as the SFRP2 receptor in retinoblastoma

(A) CXADR is highly expressed in retinoblastoma cell lines and tumors. CXADR RNA expression was analyzed by qRT-PCR and normalized to the levels in human ARPE-19 retinal pigment epithelial cells (n = 3).

(B) SFRP2 co-immunoprecipitates with endogenous CXADR in 293T cells. The indicated FLAG-tagged proteins were transfected into 293T cells, and their interaction with endogenous CXADR was assessed by anti-FLAG immunoprecipitation followed by anti-CXADR immunoblotting. C-terminally FLAG-tagged SFRP2 specifically co-immunoprecipitated with endogenous CXADR.

(C) CXADR serves as the SFRP2 receptor in retinoblastoma. C-terminally FLAG-tagged SFRP2 secreted from transfected 293T cells was incubated with Y79 cells that were

transfected with CXADR siRNA or control siRNA as indicated. Cells were washed, and the whole-cell lysate was prepared to assess the binding of SFRP2 to the cells. SFRP2-FLAG bound to control siRNA-transfected cells, and the binding was abolished by CXADR silencing. The silencing of CXADR was verified by immunoblotting.

(D) Microscale thermophoresis analysis of SFRP2-CXADR interaction. The interaction between recombinant SFRP2 (6838-FR-025, R&D Systems) and recombinant CXADR (3336-CX-05, R&D Systems) was analyzed by microscale thermophoresis, which determined the K_D of interaction to be 11.9 nM.

(E) CXADR silencing rescues growth inhibition following SFRP2 silencing. RB383 and Y79 cells were transfected with SFRP2 siRNA, CXADR siRNA, and/or control siRNA as indicated. Cell proliferation was assessed by IncuCyte.

(F) CXADR silencing abrogates CREB phosphorylation upon SFRP2 silencing. RB383 and Y79 cells were transfected with SFRP2 siRNA, CXADR siRNA, and/or control siRNA as indicated. The levels of SFRP2, CXADR, phosphorylated CREB, and tubulin were assessed by immunoblotting 48 h after transfection. A representative result from three independent experiments is shown.

(G) CXADR silencing abrogates NO production upon SFRP2 silencing. RB383 and Y79 cells were transfected with SFRP2 siRNA, CXADR siRNA, and/or control siRNA as indicated. The NO production in cell lysate was assessed 12 h and 24 h after siRNA transfection (n = 3).

(H) CXADR overexpression inhibits retinoblastoma growth. Y79 cells were infected with lentiviruses expressing CXADR or empty vector, and cell proliferation was assessed by IncuCyte. CXADR expression was verified by anti-CXADR immunoblotting (inset).

(I) CXADR overexpression results in NO production, which can be suppressed by recombinant SFRP2. NO production is enhanced in CXADR-overexpressing Y79 cells, which was rapidly suppressed by addition of recombinant SFRP2 (250 ng/mL) to the culture medium (n = 3).

(J) Growth inhibition by CXADR overexpression can be rescued by recombinant SFRP2. Y79 cells expressing CXADR or empty vector were treated with recombinant SFRP2 (250 ng/mL) or left untreated, and cell proliferation was assessed by IncuCyte.

(K) Model for the regulation of NO production and proliferation by SFRP2 and CXADR. SFRP2 is abundantly secreted from retinoblastoma, binds CXADR, and prevents NO production (1). SFRP2 silencing triggers NO production through CXADR, leading to growth arrest (2). When both SFRP2 and CXADR are silenced, NO production is not induced, and retinoblastoma can proliferate (3). CXADR silencing does not induce NO production and allows retinoblastoma proliferation (4).

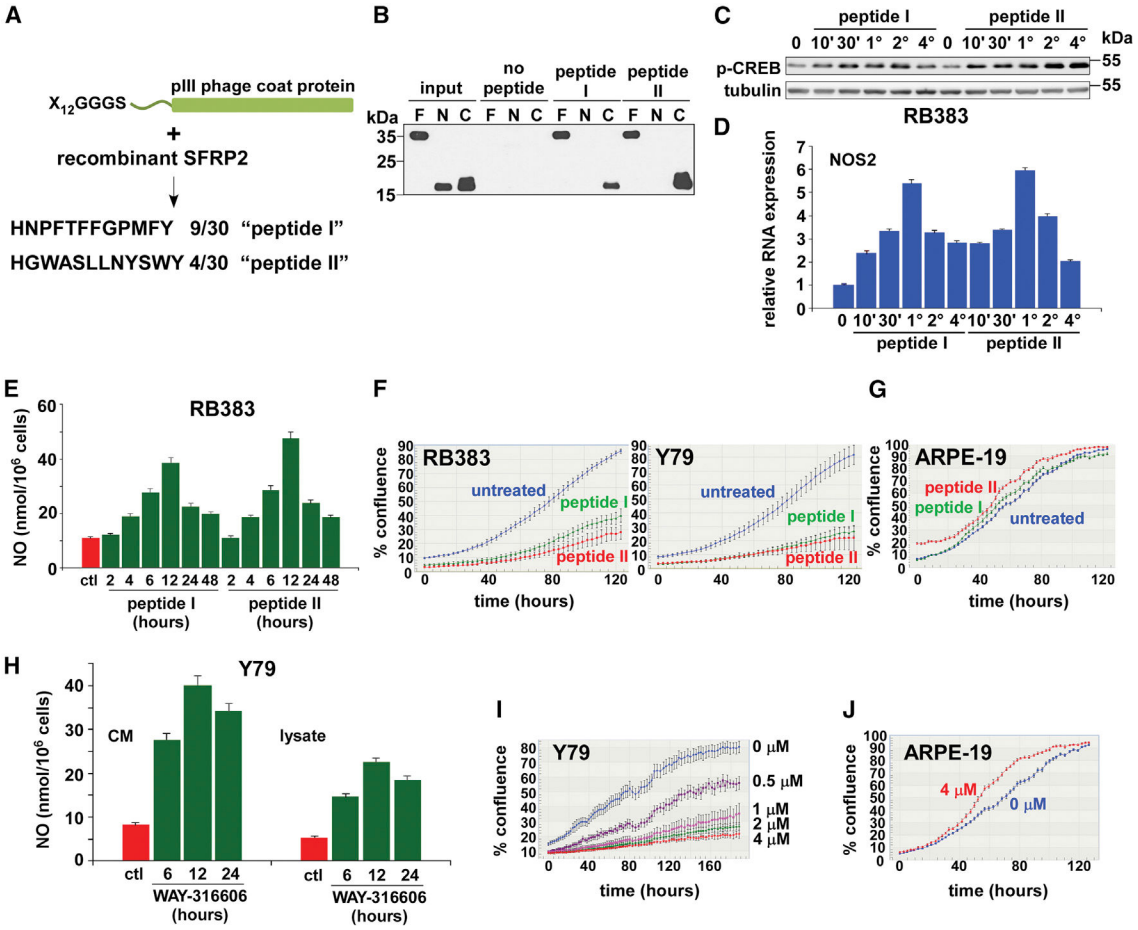

Figure 5. Targeting SFRP2 signaling in retinoblastoma

(A) Phage display library screening for SFRP2-binding peptides. The phage display library expressing random 12-mer peptides was screened with recombinant SFRP2, which led to identification of the HNPFTFFGPMFY peptide (peptide I) 9 times and the HGWASLLNYSWY peptide (peptide II) 4 times among 30 phage clones sequenced.

(B) Peptides I and II bind the SFRP2 C-terminal netrin domain. C-terminally FLAG-tagged full-length SFRP2 (F), the SFRP2 N-terminal cysteine-rich domain (1–164; N), or the SFRP2 C-terminal netrin domain (165–295 with a signal peptide at the N terminus; C) was produced in the CM of transfected 293T cells and incubated with biotinylated peptide I, peptide II, or no peptide. Streptavidin agarose pull-down followed by anti-FLAG immunoblotting detected the specific interaction of peptides I and II with full-length SFRP2 (F) and the SFRP2 C-terminal netrin domain (C). A representative result from three independent experiments is shown.

(C) SFRP2-binding peptides induce phosphorylated CREB in retinoblastoma. RB383 cells were treated with synthetic peptides I and II (1 μg/mL), and the levels of phosphorylated CREB (phospho-serine 133) at the indicated time were assessed by immunoblotting.

(D) SFRP2-binding peptides induce NOS2 in retinoblastoma. RB383 cells were treated with peptides I and II (1 μg/mL), and the RNA levels of NOS2 at the indicated time were assessed by qRT-PCR (n = 3).

(E) SFRP2-binding peptides induce NO production in retinoblastoma. RB383 cells were treated with peptides I and II (1 μg/mL), and NO production in the CM at the indicated time was analyzed by nitrite/nitrate colorimetric assays (n = 3).

(F) SFRP2-binding peptides inhibit retinoblastoma growth. RB383 and Y79 cells were treated with peptide I or II (1 μg/mL) or left untreated, and cell proliferation was assessed by IncuCyte.

(G) SFRP2-binding peptides do not inhibit the growth of retinal pigment epithelial cells. ARPE-19 cells were treated with peptides I and II (1 μg/mL) or left untreated, and cell proliferation was assessed by IncuCyte.

(H) An SFRP inhibitor, WAY-316606, induces NO production in retinoblastoma. Y79 cells were treated with 2 μM WAY-316606, and the NO production in the CM and cell lysate at the indicated time was analyzed by nitrite/nitrate colorimetric assays (n = 3).

(I) WAY-316606 suppresses retinoblastoma growth. Y79 cells were treated with the indicated concentration of WAY-316606, and cell proliferation was assessed by IncuCyte.

(J) WAY-316606 does not inhibit growth of retinal pigment epithelial cells. ARPE-19 cells were treated with 4 μM WAY-316606 or left untreated, and cell proliferation was assessed by IncuCyte.

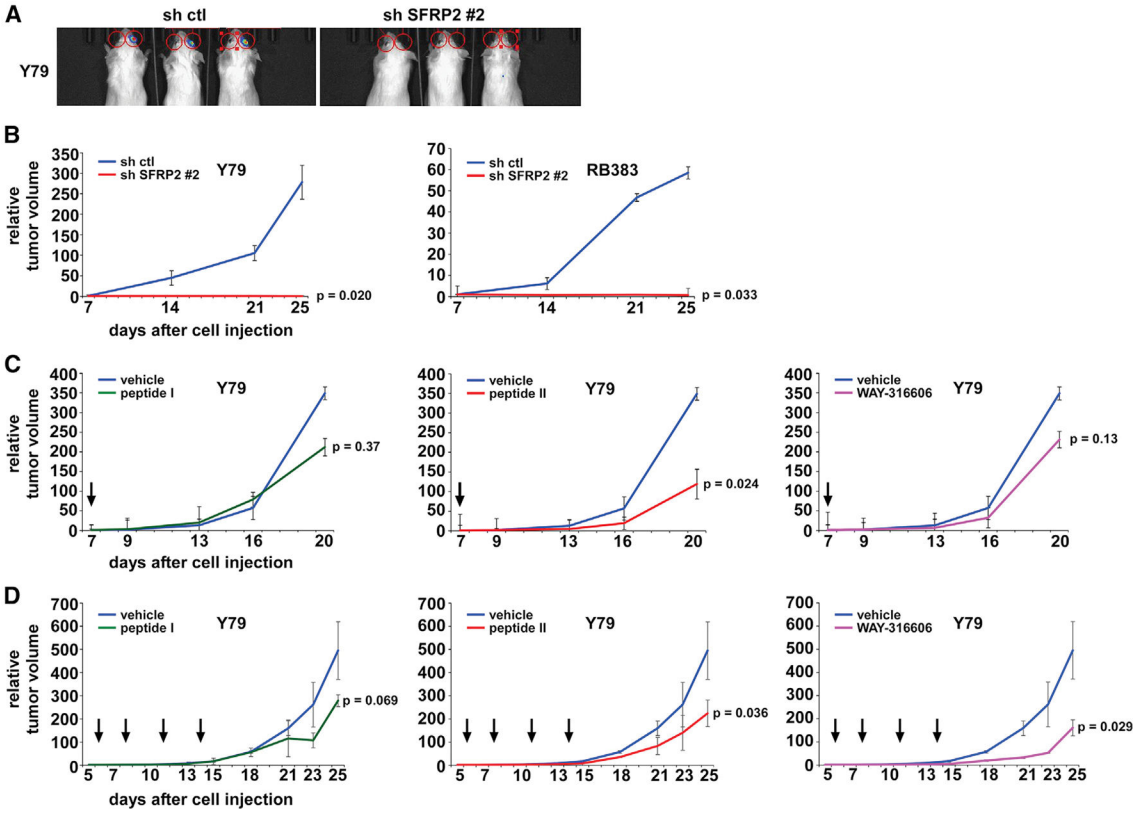

Figure 6. The effect of SFRP2 manipulation on retinoblastoma orthotopic xenograft tumor growth

(A) Bioluminescence monitoring of retinoblastoma orthotopic xenograft tumor growth. Y79 retinoblastoma cells engineered to express luciferase were infected with lentiviruses expressing SFRP2 shRNA-2 or control shRNA. After puromycin selection, retinoblastoma cells were injected into the right vitreous bodies of SCID mice, and tumor growth was monitored by Xenogen IVIS imaging system.

(B) Retinoblastoma orthotopic xenograft tumor growth depends on SFRP2. Y79 and RB383 retinoblastoma cells engineered to express luciferase were infected with lentiviruses expressing SFRP2 shRNA-2 or control shRNA. After puromycin selection, retinoblastoma cells were injected into the right vitreous bodies of SCID mice, and tumor growth was monitored by Xenogen IVIS imaging system. SFRP2 shRNA silencing abolished orthotopic tumor growth. The p values were calculated using Student's t test (two tailed). n = 3.

(C) The effect of a one-time injection of SFRP2-binding peptides I or II or WAY-316606 on orthotopic xenograft tumor growth. Y79 retinoblastoma cells engineered to express luciferase were injected into the right vitreous bodies of SCID mice. Seven days after cell injection (arrows), 3 μg of peptide I, peptide II, WAY-316606, or a vehicle was injected into the tumor-bearing vitreous bodies, and tumor growth was monitored. The p values were calculated using Student's t test (two tailed). n = 3.

(D) The effect of four-times repeated injections of SFRP2-binding peptide I or II or WAY-316606 on orthotopic xenograft tumor growth. Y79 retinoblastoma cells engineered to express luciferase were injected into the right vitreous bodies of SCID mice. Twelve micrograms of peptide I, peptide II, WAY-316606, or a vehicle was injected into the tumor-

bearing vitreous bodies 6, 8, 11, and 14 days after cell injection (arrows), and tumor growth was monitored. The p values were calculated using Student's t test (two tailed). n = 3.

KEY RESOURCES TABLE

REAGENT or RESOURCE	SOURCE	IDENTIFIER
Antibodies		
SFRP2	MyBioSource	MBS855517
SFRP2	Millipore	MABC539
SFRP2	Santa Cruz Biotechnology	sc-13940; RRID: AB_2187087
PARP	Cell Signaling Technology	9542; RRID: AB_2160739
tubulin	Developmental Studies Hybridoma Bank	E7; RRID:AB_528499
nNOS/NOS1	Cell Signaling Technology	4231; RRID:AB_2152485
iNOS/NOS2	Cell Signaling Technology	13120; RRID:AB_2687529
eNOS/NOS3	Cell Signaling Technology	32,027; RRID:AB_2728756
p21	Cell Signaling Technology	2946; RRID:AB_2260325
p53	Santa Cruz Biotechnology	sc-126; RRID:AB_628082
phospho-CREB	Cell Signaling Technology	9198; RRID:AB_2561044
CXADR	Bethyl Laboratories	A302-847A; RRID:AB_10631611
FLAG	Sigma-Aldrich	F1804; RRID:AB_262044
β-catenin	Cell Signaling Technology	9582; RRID:AB_823447
HRP-conjugated goat anti-rabbit	Cell Signaling Technology	7074; RRID:AB_2099233
HRP-conjugated goat anti-mouse	Cell Signaling Technology	7076; RRID:AB_330924
Bacterial and virus strains		
DH10B	Thermo Fisher Scientific	12,331,013
NEB® Stable Competent *E. coli*	New England Biolabs	C3040H
Biological samples		
De-identified retinoblastoma tumor RNA samples	Cooperative Human Tissue Network	N/A
Chemicals, peptides, and recombinant proteins		
Lipofectamine™ RNAiMAX Transfection Reagent	Thermo Fisher Scientific	13,778,150
puromycin dihydrochloride	MilliporeSigma	P8833
carboxy-PTIO	Cayman Chemical	81,540
L-NMMA	Cayman Chemical	10,005,031
SNAP	Cayman Chemical	82,250
NS-2028	Cayman Chemical	81,600
KT5823	Tocris Bioscience	1289
H89	Cayman Chemical	10,010,556
NKY80	Cayman Chemical	17,777
XAV939	Cayman Chemical	13,596
IWP-L6	Cayman Chemical	15,243
recombinant SFRP2	R&D systems	6838-FR-025
recombinant CXADR	R&D systems	3336-CX-050

REAGENT or RESOURCE	SOURCE	IDENTIFIER
WAY-316606	Cayman Chemical	26,324
Critical commercial assays		
Nitrate/Nitrite Colorimetric Assay Kit	Cayman Chemical	780,001
Cyclic AMP ELISA Kit	Cayman Chemical	581,001
Deposited data		
the RNA sequencing data	the GEO database	GSE161990
Y79 secretome mass spectrometry proteomics data	the PRIDE database	PXD039515
RB383 secretome mass spectrometry proteomics data	the PRIDE database	PXD039516
Y79 cell surface proteome mass spectrometry proteomics data	the PRIDE database	PXD039517
RB383 cell surface proteome mass spectrometry proteomics data	the PRIDE database	PXD039518
Experimental models: Cell lines		
Y79	ATCC	HTB-18
WERI-Rb-1	ATCC	HTB-169
RB247	Dr. Brenda Gallie	N/A
RB383	Dr. Brenda Gallie	N/A
RB409	Dr. Brenda Gallie	N/A
ARPE-19	ATCC	CRL-2302
293T	ATCC	CRL-3216
AF22	Dr. Anna Falk	N/A
Experimental models: Organisms/strains		
C.B.17SC scid$^{-/-}$ mice, 5–6 weeks old	Taconic Biosciences	CB17SC
Oligonucleotides		
SFRP2 forward, TTGAGTGCGACCGTTTCC	Thermo Fisher Scientific	N/A
SFRP2 reverse, AAGCGTTTCCATTATGTCGTTG	Thermo Fisher Scientific	N/A
CXADR forward, CTGTGCGGAGTAGTGGATTT	Thermo Fisher Scientific	N/A
CXADR reverse, GTCTTCGGGACTAAGCGTAAA	Thermo Fisher Scientific	N/A
NOS2 forward, GGAGACCCAAGAGAAGAGAGA	Thermo Fisher Scientific	N/A
NOS2 reverse, CAAAGAGGATGGTGACTCTGAC	Thermo Fisher Scientific	N/A
NOS3 forward, CATCACCAGGAAGAAGACCTTTA	Thermo Fisher Scientific	N/A
NOS3 reverse, TACAGGATTGTCGCCTTCAC	Thermo Fisher Scientific	N/A
GAPDH forward, GGTGTGAACCATGAGAAGTATGA	Thermo Fisher Scientific	N/A
GAPDH reverse, GAGTCCTTCCACGATACCAAAG	Thermo Fisher Scientific	N/A
Recombinant DNA		
pcDNA3.1 vector	Invitrogen/Thermo Fisher Scientific	V79020
pCDH1-MCS1-EF1-Puro vector	System Biosciences	CD510A-1